The phosphatase regulator NIPP1 restrains chemokine-driven skin inflammation

Iris Verbinnen[1] (0000-0002-3681-1628), Marloes Jonkhout[1] (0000-0002-6099-927X), Kifayathullah Liakath-Ali[2] (0000-0001-9047-7424), Kathelijne Szekér[1] (0000-0001-6876-1058), Mónica Ferreira[1] (0000-0001-9609-5099), Shannah Boens[1] (0000-0002-1542-0126), Raphael Rouget[1] (0000-0002-0751-851), Margareta Nikolic[1] (0000-0003-0193-4203), Susan Schlenner[3] (0000-0002-8553-3388), Aleyde Van Eynde[1$] (0000-0002-3462-4976), and Mathieu Bollen[1$] (0000-0003-4975-1510)

[1]Laboratory of Biosignaling & Therapeutics, KU Leuven Department of Cellular and Molecular Medicine, University of Leuven, Belgium; [2]Centre for Stem Cells and Regenerative Medicine, King's College London, Guy's Hospital, London, United Kingdom; [3]Laboratory of Adaptive Immunity, KU Leuven Department of Microbiology, Immunology and Transplantation, University of Leuven, Belgium

$ *Joint corresponding and last authors:*

Mathieu Bollen and Aleyde Van Eynde
KU Leuven, Campus Gasthuisberg,
Herestraat 49, O&N1, PB901,
B-3000 Leuven, Belgium.
Phone: +32-16-33 06 44
E-mail: Mathieu.Bollen@kuleuven.be and Aleyde.VanEynde@kuleuven.be

Keywords: chemokines, cytokines, inflammation, hair-follicle stem cells, NIPP1, protein phosphatase-1,

Short title: Inflammation induced by NIPP1-null keratinocytes

Abbreviations: NIPP1, nuclear inhibitor of protein phosphatase 1 (PP1); FHA, forkhead associated; IFE, interfollicular epidermis; HF, hair follicle; HFSCs, hair follicle stem cells; CTR, control; SKO, skin-specific NIPP1 knockout; TEWL, transepidermal water loss; BrdU, bromo-deoxyuridine; H3S10ph, histone H3 phosphorylated at Ser10; KRT, keratin; FLG, filaggrin; LOR, loricrin; ITG, integrin; FASN, fatty acid synthase; EdU, 5-ethynyl-2'-deoxyuridine; LRC, label-retaining-cell; FACS, fluorescence-activated-cell-sorting; DEGs, differentially expressed genes; EDC, epidermal differentiation complex; BEC, basal epidermal cell; PRC2, polycomb repressive complex 2.

ABSTRACT

NIPP1 is a ubiquitously expressed nuclear protein that regulates functions of protein Ser/Thr phosphatase-1 in cell proliferation and lineage specification. The role of NIPP1 in tissue homeostasis is not fully understood. Here we show that the selective deletion of NIPP1 in mouse epidermis resulted in epidermal hyperproliferation, a reduced adherence of basal keratinocytes and a gradual decrease in the stemness of hair follicle stem cells, culminating in hair loss. This complex phenotype was associated with chronic sterile skin inflammation and could be partially rescued by dexamethasone treatment. NIPP1-deficient keratinocytes massively expressed pro-inflammatory chemokines and immunomodulatory proteins in a cell-autonomous manner. Chemokines subsequently induced the recruitment and activation of immune cells, in particular conventional dendritic cells and Langerhans cells, accounting for the chronic inflammation phenotype. Our data identify NIPP1 as a key regulator of epidermal homeostasis and as a potential target for the treatment of inflammatory skin diseases.

INTRODUCTION

NIPP1, for nuclear inhibitor of protein phosphatase 1 (PP1), is encoded by *Ppp1r8* and is ubiquitously expressed in the nucleus of metazoan and plant cells (Ceulemans et al. 2002). The heterodimeric PP1:NIPP1 holoenzyme is inactive under steady-state but can be activated by the phosphorylation-induced allosteric removal of the C-terminal PP1-inhibitory domain of NIPP1 (Beullens et al. 2000). Activated PP1:NIPP1 selectively dephosphorylates phosphoproteins that are recruited via the N-terminal forkhead-associated (FHA) domain of NIPP1 and include such diverse proteins as protein methyltransferase EZH2, pre-mRNA splicing factors SF3B1/SAP155 and CDC5L, and protein kinase MELK (Boudrez et al. 2000; Boudrez et al. 2002; Vulsteke et al. 2004; Nuytten et al. 2008). NIPP1 has been identified as a key regulator of proliferation and lineage specification (Van Eynde et al. 2004; Boens et al. 2016; Ferreira et

al. 2017). Indeed, *Ppp1r8*$^{-/-}$ embryos suffered from a reduced cell proliferation and died at the gastrulation stage (Van Eynde et al. 2004). Likewise, the postnatal deletion of NIPP1 in testis resulted in the progressive loss of germ cells (Ferreira et al. 2017). In contrast, the deletion of NIPP1 in liver epithelial cells caused a slow-onset hyperproliferation of biliary epithelial cells (Boens et al. 2016).

Skin epidermis forms a stratified epithelium, known as interfollicular epidermis (IFE), and is associated with different appendages, including hair follicles (HFs), sebaceous glands and sweat glands (Belokhvostova et al. 2018). The epidermis and its appendages have a high cellular turnover and are maintained by different stem-cell populations (Gonzales and Fuchs 2017; Belokhvostova et al. 2018). In the IFE, stem cells give rise to proliferating keratinocytes in the basal layer. When basal keratinocytes detach, they move upwards to the suprabasal layers where they withdraw from the cell cycle and differentiate into spinous and granular keratinocytes and finally into dead corneocytes (Hänel et al. 2013). In the bulge region of the HFs, hair follicle-stem cells (HFSCs) generate progenitor cells that differentiate into the various cell lineages of the hair shaft and inner root sheath (Gonzales and Fuchs 2017). The fate of HFSCs and progenitor cells is tightly controlled by their microenvironment or niche. Skin homeostasis depends on a complex interaction between keratinocytes and other skin-resident cells, including immune cells (Heath and Carbone 2013; Kumari and Pasparakis 2017; Kabashima et al. 2019). Keratinocytes themselves can also act as innate immune cells as they can release chemokines that recruit and activate immune cells (Fritz et al. 2017; Otsuka et al. 2017; Eyerich et al. 2018). The chronic release of chemokines by keratinocytes and immune cells can cause severe inflammatory skin diseases, such as atopic dermatitis and psoriasis (Li et al. 2018).

We have generated a mouse model for the inactivation of both *Ppp1r8* alleles in keratinocytes. We report here that adult mice lacking NIPP1 in the epidermis develop a stress

response that culminates in a massive release of cytokines, the recruitment of immune cells and chronic sterile skin inflammation.

RESULTS

Epidermal-barrier dysfunction and hair loss in *Ppp1r8*$^{-/-}$ mouse skin

We selectively inactivated *Ppp1r8* in keratinocytes using CRE recombinase under control of the *Keratin-14* promoter (see Methods section). Tg*(Krt14-Cre)/Ppp1r8*$^{fl/+}$ and Tg*(Krt14-Cre)/Ppp1r8*$^{fl/-}$ were used as controls (CTR) and skin-specific NIPP1 knockout (SKO) mice, respectively (**Fig. S1a**). Immunostaining, immunoblotting and qRT-PCR revealed efficient removal of NIPP1 from the IFE and HFs in SKO tail and back (dorsal) skin (**Figs. 1a-d**).

Adult SKOs could be macroscopically distinguished from CTR mice at the age of 8 weeks by their thickened ears and a dry, flaky tail that showed patches with lost hair and coloration (**Fig. 1e**). At later ages the SKOs also showed a more global body-hair loss (alopecia) (**Fig. 1f**), and visibly suffered from pruritus and associated scratching (**Movie S1; Figs. S1b-c**). Moreover, SKOs of > 6 months often developed chronic lesions around the ears, snout and throat (**Fig. 1g**). These lesions did not appear to be caused by a deficiency in wound-healing as no differences were noted between CTRs and SKOs in the healing efficiency of 5-mm punch biopsies on the back skin (**Figs. S1d-e**). Both CTR and SKO embryos stained with toluidine blue at E16.5, but not at E18.5 (**Fig. S1f**), demonstrating that deletion of NIPP1 did not affect the establishment of the embryonic epidermal barrier. Interestingly, transepidermal-water-loss (TEWL) assays in adult mice revealed a nearly two-fold increased water loss in SKOs (**Fig. 1h**), indicating epidermal-barrier dysfunction.

Epidermal hyperplasia in the SKOs

Histological analysis identified increased epidermal thickness (acanthosis) in both tail (**Fig. 2a**) and back skin (**Fig. S2a**) of SKO mice at the age of 8 weeks and 9 months, respectively.

Acanthosis in the SKO tails was associated with hyperproliferation of cells in the basal layer, as demonstrated by a twofold higher incorporation of bromo-deoxyuridine (BrdU) during a 4h-pulse labeling (**Fig. 2b**), and similarly elevated levels of Ki67 (**Fig. 2c**) and histone H3 phosphorylated at Ser10 (H3S10ph) (**Fig. 2d**). The back skin of 8-week-old SKOs also contained more BrdU-positive cells in the IFE (**Fig. S2b**). In further agreement with a hyperproliferation phenotype (Liakath-Ali et al. 2014), the basal-cell marker Keratin-14 (KRT14) was also expressed in the suprabasal layers (**Fig. S2c**). Moreover, the suprabasal layers were expanded, as demonstrated by stainings for the spinous-layer specific markers Keratin-10 (KRT10) and Keratin-1 (KRT1) (**Figs. 2e-f**), and the granular-layer specific markers Filaggrin (FLG) and Loricrin (LOR) (**Figs. 2g-h**). These observations were validated by qRT-PCR analysis (**Figs. S2d-g**). In back skin, the thickness of the KRT14-layer, but not the FLG layer, was increased in SKO mice of 8 weeks (**Fig. S2h**). Since hyperproliferation is generally associated with reduced adherence of keratinocytes to the basement membrane, we quantified the expression of integrins, which link the keratin intermediate filaments to the extracellular matrix. The level of integrins ITGA6 and ITGB4 in tail skin was decreased by 40% and 60%, respectively, in the SKOs, as deduced from immunostainings (**Figs. 2i-j**) and qRT-PCRs (**Fig. S2i**), suggesting a reduced engagement of NIPP1-null keratinocytes to laminins in the extracellular matrix. This finding is consistent with the presence of basal cells in the suprabasal layers (**Fig. S2c**) and an increased TEWL (**Fig. 1h**). In addition to these *in vivo* experiments, we also examined the effect of NIPP1 depletion on the proliferation of cultured human keratinocytes (HaCaT). Both MTT and viability assays (IncuCyte) showed a decreased growth rate after the siRNA-mediated knockdown of NIPP1 (**Figs. S2j-k**). The IncuCyte scratch wound assay showed that NIPP1 depletion delayed the migration of HaCaT cells into the created wound but, eventually, the wound healed completely (**Figs. S2l-m**). We conclude that NIPP1 deletion reduces the proliferation and migratory capacity of HaCaT cells. This is opposite to

what we observed for keratinocytes in the SKOs and suggests that the response to a depletion of NIPP1 is context-dependent and affected, for example, by other (epi)dermal cell types.

Reduced stemness and adherence of HFSCs in the SKOs

Tail epidermal wholemounts of SKOs showed loss of scales (**Fig. 3a**), aberrations in HF arrangement (**Fig. 3b**) and alterations in HF-bulge morphology (**Fig. 3c**). Indeed, the arrangement of HFs in triplets was distorted in SKO tails (**Fig. 3b**), but the total number of HFs was not significantly altered (**Fig. S3a**). Immunostaining of tail wholemounts revealed that bulges (KRT15-positive) were absent or less organized in NIPP1-deficient HFs (**Fig. 3c**). However, the infundibulum (**Fig. 3c**) and associated sebaceous glands (FASN-positive) were always visible in the SKO tail (**Fig. 3d**). Quantification of Ki67-staining in the wholemounts also showed an increased proliferation of cells in SKO HFs (**Fig. 3e**). In addition, co-immunostaining of CD34 and Ki67 demonstrated hat HFSCs (CD34-positive) in the SKOs were more proliferative in the telogen phase of the hair cycle (**Fig. 3f**). The bulge HFSCs are required to maintain and renew HFs and also produce the cells of the keratinized hair shaft. We hypothesized that the hair phenotype in the SKOs is (partially) explained by a loss or dysfunction of HFSCs. Consistent with this notion, we found that the expression of various HFSC markers was substantially decreased in SKO tail epidermis (**Fig. 3g**), and these differences further increased with age (**Fig. S3b**). Furthermore, immunostaining for the HFSC markers SOX9 and CD34 confirmed a reduced number of HFSCs in SKO tail (**Figs. 3h and S3c**) and back skin (**Fig. S3d**). Also, the number of EdU label-retaining-cells (LRCs) following a chase period of 77 days (**Fig. S3e**) was severely reduced in HFs of the SKO tail (**Fig. 3i**) and back skin (**Fig. S3f**). This is indicative for a loss of slow-cycling stem cells (Fuchs 2009; Kretzschmar and Watt 2014), which likely stems from hyperproliferation-induced exhaustion of HFSCs (**Fig. 3f**). Finally, we used fluorescence-activated cell sorting (FACS) to isolate HFSCs ($CD34^{high}$/$ITGA6^{high}$) from CTR and SKO tail epidermis (**Fig. S3g**). The number of

HFSCs in the SKOs was reduced by some 40%, as quantified by cell-sorting analysis (**Fig. S3h**). Moreover, qRT-PCR analysis of the $CD34^{high}/ITGA6^{high}$ cell population (HFSCs) revealed that HFSC markers, such as *Sox9, Nfatc1*, *Lhx2*, *Dkk3* and *Fzd2,* and the cell-adhesion markers *Itgb1*, *Itgb4* and *Itga6* were significantly reduced in purified HFSCs of the SKOs, suggesting that NIPP1-deficient HFSCs had lost factors essential for stemness and displayed a reduced matrix adherence (**Fig. 3j**). Collectively, these data demonstrated that NIPP1 deletion resulted in a reduction of HFSCs with the remaining HFSCs displaying reduced stemness and cell adherence, consistent with the observed hair-loss phenotype.

The overt SKO phenotype stems from a chemokine-driven sterile inflammatory response

SKO tail and back (epi)dermis showed an increased infiltration of leucocytes, as demonstrated by staining for CD45+ cells (**Figs. 4a and S4a**) and flow cytometry (**Fig. 4b**). CD117-staining disclosed an increased number of mast cells in SKO tail skin (**Fig. S4b**). We quantified immune-cell types by flow cytometry and found that SKO tail skin contained more antigen-presenting cells, including conventional dendritic cells and Langerhans cells, but not macrophages (**Fig. 4c**). FACS analysis did not reveal biologically meaningful differences in T-cell development and homeostasis in thymus and spleen at the age of 4 weeks (**Fig. S4c**) and 8-12 weeks (**Fig. S4d**), making a contribution of these organs to the observed SKO immune response unlikely. Also, Gram and Periodic Acid Schiff (PAS) stainings were negative (data not shown), indicating that the immune response in the SKOs was not elicited by bacterial or fungal infections, respectively, but caused by pathogen-free or sterile inflammation.

To delineate the contribution of leucocytes to the SKO phenotype, we treated 6-week-old CTR and SKO mice daily, for two weeks, with either vehicle or the immune-suppressant dexamethasone (**Fig. 5a**). Strikingly, the hyperproliferation of keratinocytes in the IFE of the SKOs was reversed by this treatment, as deduced from immunostainings for H3S10ph (**Fig. 5b**). Furthermore, the reduced expression of the integrin *Itga6* (**Fig. 5c**) and the HFSC marker

Krt15 (**Fig. 5d**) were also alleviated by the dexamethasone treatment. The reduced expression of the integrin *Itgb1* was not significantly rescued (**Fig. 5c**). Together, these data suggest that epidermal hyperproliferation in the SKOs as well as the loss and reduced adherence of the HFSCs are, at least partially, caused by chronic sterile skin inflammation.

To obtain insights into the molecular signaling pathway(s) that are affected by the deletion of NIPP1, we performed a comparative transcriptome analysis (RNA-seq) on tail epidermis of CTR and SKO mice (**Fig. 5e**). In total, 846 protein-encoding genes were differentially expressed (FDR < 0.01, two-fold cut-off) (**Table S4**). The 61% differentially expressed genes (DEGs) that were downregulated in the SKOs were strongly enriched for genes encoding keratins or keratin-associated proteins (**Figs. S5a-c; Table S5**), consistent with aberrant HF development and associated hair loss. The 39% DEGs that were upregulated in the SKOs were mostly enriched for the Gene Ontology entries 'Immune_System_Process', 'Extracellular_Space' and 'Cytokine_Activity' (**Fig. S5d; Table S6**). We noted a strong upregulation of different types of cytokines in tail epidermis (**Fig. 5f**), which was confirmed by qRT-PCR (**Fig. S5e**). In fact, the chemokine *Ccl2* was the most upregulated gene (> 40-fold), and the chemokines *Ccl1*, *Ccl20*, *Cxcl10* and *Cxcl9* were at least 8 times more expressed in SKO epidermis (**Table S4 and S6**). Other immunomodulatory genes, including extracellular matrix proteins (**Fig. 5g**) or antimicrobial peptides, such as S100 proteins and β-defensins (**Fig. 5h**), were also upregulated in the SKOs. The chemokines *Ccl1* and *Ccl2* were also upregulated in back epidermis (8 weeks), albeit to a lesser extent (**Fig. S5f**).

Differential RNA-seq analysis also disclosed prominent changes in the expression of many genes of the Epidermal-Differentiation-Complex (EDC) locus, which encodes proteins that are essential for the terminal differentiation of keratinocytes (**Fig. S5g**) (Poterlowicz et al. 2017). The transcript level of 17 EDC genes was increased in the SKOs, while 5 genes were less expressed (**Fig. S5h**). Interestingly, genes that contribute to terminal epidermal differentiation

(e.g. *S100a8/a9,* various *Lce* genes*)* generally showed an increased expression. In contrast, genes that are expressed in HFs (*S100a3, Tchh, Tchhl1, Crnn*), and contribute to terminal hair differentiation, were downregulated in the SKOs. Collectively, the DEGs independently confirmed an increased epidermal differentiation and diminished development of the hair lineage in the SKOs, and suggested that the observed inflammatory phenotype in the SKOs is chemokine-driven.

Inflammation in the SKOs is initiated by keratinocyte-derived chemokines

Since keratinocytes as well as resident and recruited immune cells in the skin can produce cytokines, we explored the cellular source of increased cytokine expression in the SKOs. For this purpose, we isolated basal epidermal cells (BECs; CD34-neg/ITGA6^{high}) and HFSCs (CD34^{high}/ITGA6^{high}) from the epidermis of CTR and SKO tails by FACS (**Fig. 6a**). qRT-PCR analysis revealed a massive increase in the expression of cytokines, including *Ccl1*, *Ccl2*, *Cxcl1*, *Cxcl2* and *Tnf*, in the purified SKO cell populations (**Figs. 6b-c; Fig. S6a-c**). In general, the relative expression of these cytokines was higher in SKO HFSCs and BECs than in SKO epidermis. Interestingly, cytokine expression by *Ppp1r8*$^{-/-}$ keratinocytes was not affected by a prolonged treatment with dexamethasone (**Figs. 6d-e**) which did, however, partially suppress the global SKO phenotype (**Figs. 5b-d**). It should be taken into account that the dexamethasone treatment was started at 6 weeks when the phenotype was largely established, including the recruitment of immune cells. Together, these data suggested that the expression of chemokines in NIPP1-deficient keratinocytes was not caused by the observed sterile inflammatory response but the consequence of endogenous stress signaling. We proceeded to analyze cytokine expression and immune infiltration in tail epidermis of SKO mice of different ages. The deletion of NIPP1 from pre-adult SKO epidermis was confirmed by qRT-PCR (**Fig. S6d**). We already detected a small but significant increase in the expression of the chemokines *Ccl1* and *Ccl2* in SKOs of 10 and 20 days, respectively (**Figs. 6f-g**). In contrast, the induction of other

immunoregulatory genes, such as *S100a8* and *Mmp9*, was only detected from 28 days onwards (**Figs. 6h and S6e**). The immune infiltration was evaluated in both epidermis and dermis by examining the level of *Cd45* transcripts. The increased level of *Cd45* transcripts was only detected from 20 days onwards in the dermis (**Fig. S6f**) and from 28 days in epidermis (**Fig. 6i**). Finally, the cell-autonomous character of cytokine secretion by NIPP1-depleted keratinocytes was independently validated by our observation that cultured human HaCaT keratinocytes also secrete cytokines after the siRNA-mediated knockdown of NIPP1 (**Fig. 6j**), albeit to a lesser extent than observed for *Ppp1r8*$^{-/-}$ mouse keratinocytes. Altogether, these data suggested that NIPP1-null keratinocytes release cytokines, including CCL1/2, in a cell-autonomous manner from an age of ~10 days onwards (**Fig. 6k**). CCL1/2, and other cytokines, act as chemoattractant for immune cells, in particular dendritic cells that express the corresponding chemokine receptors. Activated immune cells subsequently release additional cytokines that contribute to the observed sterile inflammatory response and SKO phenotype at later ages.

DISCUSSION

We have shown that *Ppp1r8*$^{-/-}$ keratinocytes spontaneously and constitutively release chemokines that attract immune cells and induce a chronic sterile inflammatory response. Both HFSCs and BECs purified from SKOs showed a vastly increased expression of pro-inflammatory chemokines (**Fig. 6**). This increased chemokine expression was not affected by a prolonged treatment with an immunosuppressant and was also detected in cultured HaCaT keratinocytes, following the siRNA-mediated knockdown of NIPP1, confirming the cell-autonomous and inflammation-independent nature of this response. Importantly, the increased expression of chemokines in the SKO epidermis preceded the recruitment of immune cells to

the skin by 1-2 weeks, demonstrating that the initial trigger for the inflammatory response was not provided by recruited immune cells (**Figs. 6 and S6f**).

Inflammation is a protective response aimed at removing the causes of cell stress (e.g. infection), clearing damaged cells and initiating tissue repair (Karin and Clevers 2016). However, when the cause of stress is not well-resolved, the inflammation becomes chronic and can lead to tissue destruction and pathologies such as psoriasis and atopic dermatitis (Rotty and Coulombe 2012; Lessard et al. 2013). Consistent with a chronic-inflammation phenotype the skin of the SKOs displayed properties of both tissue repair and destruction. On the one hand the epidermis of SKOs was hyperplastic (**Fig. 2**) and showed an increased expression of epithelial keratins and terminal-epidermal-differentiation genes (**Fig. S5**). On the other hand, the HFSCs of the SKOs were hyperproliferative and showed a decreased stemness and adherence, accounting for the degeneration of HFs (**Fig. 3**), hair loss and the gradual appearance of skin wounds (**Fig. 1**). Importantly, the SKO phenotype was partially rescued by the repeated administration of an immunosuppressant (**Fig. 5**), indicating that it was caused by chronic inflammation. At first glance, the SKO phenotype is reminiscent of the hepatic response to the deletion of NIPP1 in hepatoblast-derived epithelial cells, which also involved both a hyperplastic and inflammatory response (Boens et al. 2016). However, inflammation in *Ppp1r8*$^{-/-}$ livers developed much later than the hyperproliferation of bile-duct progenitor cells, arguing against a causal relationship.

Inflammation-induced epidermal hyperproliferation, as elicited in the NIPP1 SKOs, is well understood and is mainly mediated by increased signaling through the NF-κB pathway (Liu et al. 2017). However, the mechanism underlying the degeneration of HFs in the SKOs is less clear and can involve multiple mechanisms. HFs normally escape immune surveillance but the deletion of NIPP1 somehow results in the loss of their 'immune privilege' status, making the HSFCs accessible to removal by immune cells (Azzawi et al. 2018). HFSCs are also known to

be extremely sensitive to stress-signaling, which causes their differentiation and migration out of the stem-cell niche (Schuler et al. 2018). It is therefore possible that the activation of a stress-signaling pathway, induced by the absence of NIPP1 (see below), accounts for the differentiation and loss of HFSCs in the SKOs. Importantly, HFs can also degenerate in an inflammation-independent manner, for example by depletion of core components of the Polycomb Repressive Complex 2, including EZH1/2 (Ezhkova et al. 2011), an established substrate of PP1:NIPP1 (Minnebo et al. 2013). Since HF degeneration in the SKOs was only partially rescued by a dexamethasone treatment (**Fig. 5**), it cannot be excluded that HF degeneration in the SKOs is (partially) inflammation-independent and due to decreased PRC2-mediated signaling.

It is not yet clear how NIPP1 regulates the expression of cytokines in keratinocytes. Since NIPP1 recruits phosphoproteins for regulated dephosphorylation by associated PP1, we speculate that NIPP1 controls the phosphorylation of transcription factors and/or transcriptional co-repressors/activators that regulate the expression of cytokine genes. Consistent with this view, it has been shown that NIPP1 controls the phosphorylation status and activity of the transcriptional co-repressors Enhancer of Zeste Homolog 2 (EZH2) and Krüppel-associated box domain-associated protein 1 (KAP1) (Ferreira et al. 2018; Minnebo et al. 2013; Smith-Moore et al. 2018). Since many of cytokine genes with an altered expression in the SKOs have NF-κB binding sites in their promoters, NIPP1 may affect cytokine expression through PP1-mediated dephosphorylation of NF-κB (Richmond 2002; Taniguchi and Karin 2018). In addition, NIPP1 may function itself as a transcription factor, as suggested by a genome-wide promoter binding profiling of NIPP1 in HeLa cells using the DamID technique (Verheyen et al. 2015). Interestingly, the latter approach identified the *Cxcl1* promoter, as well as the *Krtap19-4* and *Krtap19-5* promoters, as putative binding sites for NIPP1.

Currently it is not clear which stress pathway is deregulated in keratinocytes following the depletion of NIPP1 and leads to an increased expression of cytokines. The stable expression of a PP1-NIPP1 fusion in HeLa cells resulted in the accumulation of DNA damage, R-loops and hypercondensed chromatin, and was associated with a reduced DNA-repair capacity (Winkler et al. 2018). Conversely, the deletion of NIPP1 in skin or liver increased the repair-capacity of DNA damage induced by mutagens, which correlated with an increased expression of key DNA-repair proteins (unpublished data). The exact role of PP1:NIPP1 in DNA-damage and -repair signaling is not yet understood but we speculate that it involves the (de)phosphorylation of substrates since the effects of a PP1-NIPP1 fusion on DNA damage were dependent on a functional substrate-binding FHA-domain and an active PP1 moiety (Winkler et al. 2018). Interestingly, all known substrates of PP1:NIPP1 have been implicated in DNA damage or repair signaling (Maréchal et al. 2014; Savage et al. 2014; Beke et al. 2015; Rondinelli et al. 2017), suggesting that the phenotype of the NIPP1 SKOs may be caused by an altered phosphorylation status of PP1:NIPP1 substrates.

In conclusion, we have shown that deletion of NIPP1 in keratinocytes triggers the release of cytokines, which unleashes a chronic inflammatory response and culminates in a pathological phenotype that is reminiscent of human inflammatory skin diseases such as atopic dermatitis and psoriasis. It will be interesting to investigate whether the activation of PP1:NIPP1, for example with compounds that disrupt the interaction of the C-terminal inhibitory domain of NIPP1 with PP1, alleviate the development of these inflammatory skin diseases in various models.

MATERIALS AND METHODS

Animals

Mice were housed in a pathogen-free animal facility under standard 12h-light/dark cycles with water and chow *ad libitum*. The generation of skin-specific NIPP1 KO and CTR mice is

described in Supplementary Materials and Methods. All experimental protocols were in accordance with and approved by the Guide of Care of Experimental Animals of the KU Leuven Ethical Committee (license number 053/2018).

Mouse treatments

Pups of 10 days were intraperitoneally injected with 100 µl of 6.25 mg/ml 5-ethynyl-2'-deoxyuridine (EdU) every 12 hours for a total of 4 injections and imaged using the Click-iT® EdU Alexa Fluor® 488 Imaging Kit (Thermo Fisher Scientific). Skin samples were collected 77 days after the last injection. Mice were intraperitoneally injected daily, for 15 consecutive days, with 4 mg/kg rapidexon/dexamethasone (Eurovet Animal Health, Dechra) or vehicle (saline). The skin-barrier assays, i.e. embryo whole-mount dye-penetration assays and transepidermal water loss; the assessment of scratching behavior and the wound-healing assays are detailed described in Supplementary Material and Methods.

Flow cytometry

HFSCs and BECs, immune cells in the skin, and T cell maturation and activation in spleens and thymi were analysed by flow cytometry as detailed in Supplementary Materials and Methods.

RNA-sequencing and qRT-PCR

Total RNA was isolated from snap-frozen mouse epidermis, dermis, FACS-purified HFSCs and BECs or from HaCaT cells (stored at -80°C). For RNA-sequencing, total RNA was isolated from snap-frozen tail epidermis from 4 CTR and 4 SKO mice (age of 8 weeks). qRT-PCR and RNA sequencing is further described in Supplementary Materials and Methods.

Biochemical procedures and (immuno)histochemical analysis

Total lysates were made from tail epidermis and subjected to Western blot analyses as detailed in Supplementary Materials and Methods. Skin tissue was fixed and used for

(immuno)histochemical analysis according to standard protocols. All antibodies are listed in Supplementary Table S2. See also Supplementary Materials and Methods.

Cell culture

HaCaT cells were cultured in DMEM medium with 4.5 g/L glucose and 2 mM L-glutamine (Sigma-Aldrich), supplemented with 1 mM sodium pyruvate (Sigma-Aldrich), 10% FCS and 1% Penicillin/Streptomycin. The siRNA transfections were performed using RNAiMAX transfection reagent (Thermo Fisher Scientific). Knockdowns were verified by qPCR analysis of *Ppp1r8* expression. See also Supplementary Materials and Methods.

Data analysis

The results are expressed as means ± standard deviation (SD) and analyzed with the unpaired Student t-test. Statistical analysis was performed in GraphPad Prism version 7 (GraphPad software, Inc). See also Supplementary Materials and Methods.

DATA AVAILABILITY

Gene expression data are available at GEO under accession number at https://www.ncbi.nlm.nih.gov/geo/query/acc.cgi?acc=GSE116844).

CONFLICT OF INTEREST

The authors state no conflict of interest.

FUNDING

This work was supported by the Belgian Foundation Against Cancer, FWO grant G078717N, a KU Leuven BOF-grant (GOA/15/016), and NIH grant 1R01CA188382-01. Iris Verbinnen was a research fellow of the FWO Flanders.

ACKNOWLEDGEMENTS

Maud De Meyer, Fabienne Withof, Annemie Hoogmartens and Lies Pauwels provided expert technical assistance. Mieke Anthonissen is acknowledged for expert advice on TEWL assays, and Pier Andrée Pentilla, Christèle Nkama and Pradeep Kumar (https://gbiomed.kuleuven.be/english/corefacilities/facs) for FACS sorting. We thank Dr. Fiona M. Watt (King's College London) for allowing the wholemount stainings to be performed in her laboratory and for giving feedback on the data. Prof. W. Birchmeier (Max-Delbrueck-Center for Molecular Medicine, Germany) is acknowledged for the donation of Tg (Krt14-Cre) mice. Rekin's Janky of the Nucleomics Core at KU Leuven analyzed the RNA-seq data.

CRediT STATEMENT

Conceptualization, I.V., K.L., K.S., A.V.E., M.B.; Methodology, I.V., and M.J.; Validation, I.V., and M.J., Formal analysis and Investigation, I.V., M.J., K.L., K.S., M.F., S.B., R.R., M.N., S.S.; Writing – original draft, I.V., A.V.E. and M.B.; Writing – Review & Editing, I.V., K.L., S.S., A.V.E., M.B.; Supervision, A.V.E., and M.B.; Project Administration, M.B.; Funding Acquisition, A.V.E., and M.B.

REFERENCES

Azzawi S, Penzi LR, Senna MM. Immune Privilege Collapse and Alopecia Development: Is Stress a Factor. Ski. Appendage Disord. 2018. p. 236–44

Beke L, Kig C, Linders JTM, Boens S, Boeckx A, van Heerde E, et al. MELK-T1, a small-molecule inhibitor of protein kinase MELK, decreases DNA-damage tolerance in proliferating cancer cells. Biosci. Rep. 2015;35(6):e00267–e00267

Belokhvostova D, Berzanskyte I, Cujba AM, Jowett G, Marshall L, Prueller J, et al. Homeostasis, regeneration and tumour formation in the mammalian epidermis. Int. J. Dev. Biol. 2018;62(6–8):571–82

Beullens M, Vulsteke V, Van Eynde A, Jagiello I, Stalmans W, Bollen M. The C-terminus of NIPP1 (nuclear inhibitor of protein phosphatase-1) contains a novel binding site for protein phosphatase-1 that is controlled by tyrosine phosphorylation and RNA binding. Biochem. J. 2000;352 Pt 3:651–8

Boens S, Verbinnen I, Verhulst S, Szekér K, Ferreira M, Gevaert T, et al. Brief Report: The Deletion of the Phosphatase Regulator NIPP1 Causes Progenitor Cell Expansion in the Adult Liver. Stem Cells. 2016;34(8):2256–62

Boudrez A, Beullens M, Groenen P, Van Eynde A, Vulsteke V, Jagiello I, et al. NIPP1-mediated interaction of protein phosphatase-1 with CDC5L, a regulator of pre-mRNA splicing and mitotic entry. J. Biol. Chem. 2000;275(33):25411–7

Boudrez A, Beullens M, Waelkens E, Stalmans W, Bollen M. Phosphorylation-dependent interaction between the splicing factors SAP155 and NIPP1. J. Biol. Chem. 2002;277(35):31834–41

Ceulemans H, Stalmans W, Bollen M. Regulator-driven functional diversification of protein phosphatase-1 in eukaryotic evolution. BioEssays. 2002. p. 371–81

Eyerich S, Eyerich K, Traidl-Hoffmann C, Biedermann T. Cutaneous Barriers and Skin Immunity: Differentiating A Connected Network. Trends Immunol. 2018. p. 315–27

Van Eynde A, Nuytten M, Dewerchin M, Schoonjans L, Keppens S, Beullens M, et al. The Nuclear Scaffold Protein NIPP1 Is Essential for Early Embryonic Development and Cell Proliferation. Mol Cell Biol. 2004;24:5863–74

Ezhkova E, Lien WH, Stokes N, Pasolli HA, Silva JM, Fuchs E. EZH1 and EZH2 cogovern

histone H3K27 trimethylation and are essential for hair follicle homeostasis and wound repair. Genes Dev. 2011;25(5):485–98

Ferreira M, Boens S, Winkler C, Szekér K, Verbinnen I, Van Eynde A, et al. The protein phosphatase 1 regulator NIPP1 is essential for mammalian spermatogenesis. Sci. Rep. 2017;7(1)

Ferreira M, Verbinnen I, Fardilha M, Van Eynde A, Bollen M. The deletion of the protein phosphatase 1 regulator NIPP1 in testis causes hyperphosphorylation and degradation of the histone methyltransferase EZH2. J. Biol. Chem. American Society for Biochemistry and Molecular Biology; 2018;293(47):18031–9

Fritz Y, Klenotic PA, Swindell WR, Yin ZQ, Groft SG, Zhang L, et al. Induction of Alternative Proinflammatory Cytokines Accounts for Sustained Psoriasiform Skin Inflammation in IL-17C+IL-6KO Mice. J. Invest. Dermatol. 2017;137(3):696–705

Fuchs E. The Tortoise and the Hair: Slow-Cycling Cells in the Stem Cell Race. Cell. 2009. p. 811–9

Gonzales KAU, Fuchs E. Skin and Its Regenerative Powers: An Alliance between Stem Cells and Their Niche. Dev. Cell. 2017;43(4):387–401

Hänel KH, Cornelissen C, Lüscher B, Baron JM. Cytokines and the skin barrier. Int. J. Mol. Sci. 2013. p. 6720–45

Heath WR, Carbone FR. The skin-resident and migratory immune system in steady state and memory: Innate lymphocytes, dendritic cells and T cells. Nat. Immunol. 2013. p. 978–85

Kabashima K, Honda T, Ginhoux F, Egawa G. The immunological anatomy of the skin. Nat. Rev. Immunol. 2019.

Karin M, Clevers H. Reparative inflammation takes charge of tissue regeneration. Nature. 2016. p. 307–15

Kretzschmar K, Watt FM. Markers of epidermal stem cell subpopulations in adult mammalian skin. Cold Spring Harb. Perspect. Med. 2014;4(10)

Kumari S, Pasparakis M. Epithelial cell death and inflammation in skin. Curr. Top. Microbiol. Immunol. 2017. p. 77–93

Lessard JC, Pina-Paz S, Rotty JD, Hickerson RP, Kaspar RL, Balmain A, et al. Keratin 16 regulates innate immunity in response to epidermal barrier breach. Proc. Natl. Acad. Sci.

2013;110(48):19537–42

Liakath-Ali K, Vancollie VE, Heath E, Smedley DP, Estabel J, Sunter D, et al. Novel skin phenotypes revealed by a genome-wide mouse reverse genetic screen. Nat. Commun. 2014;5

Li H, Yao Q, Mariscal AG, Wu X, Hülse J, Pedersen E, et al. Epigenetic control of IL-23 expression in keratinocytes is important for chronic skin inflammation. Nat. Commun. 2018;

Liu T, Zhang L, Joo D, Sun SC. NF-κB signaling in inflammation. Signal Transduct. Target. Ther. 2017.

Maréchal A, Li JM, Ji XY, Wu CS, Yazinski SA, Nguyen HD, et al. PRP19 Transforms into a Sensor of RPA-ssDNA after DNA Damage and Drives ATR Activation via a Ubiquitin-Mediated Circuitry. Mol. Cell. 2014;53(2):235–46

Minnebo N, Görnemann J, O'Connell N, Van Dessel N, Derua R, Vermunt MW, et al. NIPP1 maintains EZH2 phosphorylation and promoter occupancy at proliferation-related target genes. Nucleic Acids Res. 2013;41(2):842–54

Nuytten M, Beke L, Van Eynde A, Ceulemans H, Beullens M, Van Hummelen P, et al. The transcriptional repressor NIPP1 is an essential player in EZH2-mediated gene silencing. Oncogene. 2008;27(10):1449–60

Otsuka A, Nomura T, Rerknimitr P, Seidel JA, Honda T, Kabashima K. The interplay between genetic and environmental factors in the pathogenesis of atopic dermatitis. Immunol. Rev. 2017. p. 246–62

Poterlowicz K, Yarker JL, Malashchuk I, Lajoie BR, Mardaryev AN, Gdula MR, et al. 5C analysis of the Epidermal Differentiation Complex locus reveals distinct chromatin interaction networks between gene-rich and gene-poor TADs in skin epithelial cells. PLoS Genet. 2017;13(9)

Richmond A. NF-κB, chemokine gene transcription and tumour growth. Nat. Rev. Immunol. 2002. p. 664–74

Rondinelli B, Gogola E, Yücel H, Duarte AA, Van De Ven M, Van Der Sluijs R, et al. EZH2 promotes degradation of stalled replication forks by recruiting MUS81 through histone H3 trimethylation. Nat. Cell Biol. 2017;19(11):1371–8

Rotty JD, Coulombe PA. A wound-induced keratin inhibits Src activity during keratinocyte migration and tissue repair. J. Cell Biol. 2012;197(3):381–9

Savage KI, Gorski JJ, Barros EM, Irwin GW, Manti L, Powell AJ, et al. Identification of a BRCA1-mRNA Splicing Complex Required for Efficient DNA Repair and Maintenance of Genomic Stability. Mol. Cell. 2014;54(3):445–59

Schuler N, Timm S, Rübe CE. Hair Follicle Stem Cell Faith Is Dependent on Chromatin Remodeling Capacity Following Low-Dose Radiation. Stem Cells. 2018;36(4):574–88

Smith-Moore S, Neil SJD, Fraefel C, Linden RM, Bollen M, Rowe HM, et al. Adeno-associated virus Rep proteins antagonize phosphatase PP1 to counteract KAP1 repression of the latent viral genome. Proc. Natl. Acad. Sci. 2018;115(15):E3529–38

Taniguchi K, Karin M. NF-B, inflammation, immunity and cancer: Coming of age. Nat. Rev. Immunol. 2018. p. 309–24

Verheyen T, Görnemann J, Verbinnen I, Boens S, Beullens M, Van Eynde A, et al. Genome-wide promoter binding profiling of protein phosphatase-1 and its major nuclear targeting subunits. Nucleic Acids Res. 2015;43(12)

Vulsteke V, Beullens M, Boudrez A, Keppens S, Van Eynde A, Rider MH, et al. Inhibition of Spliceosome Assembly by the Cell Cycle-regulated Protein Kinase MELK and Involvement of Splicing Factor NIPP1. J. Biol. Chem. 2004;279(10):8642–7

Winkler C, Rouget R, Wu D, Beullens M, Van Eynde A, Bollen M. Overexpression of PP1–NIPP1 limits the capacity of cells to repair DNA double-strand breaks. J. Cell Sci. 2018;131(13):jcs214932

FIGURE LEGENDS

Figure 1. Macroscopic phenotype associated with the inactivation of *Ppp1r8* in mouse skin.

(a) NIPP1 immunostains (green) in longitudinal sections of tail and back skin from CTRs and SKOs at 8 weeks (tail) and 4 weeks (back). Dapi (blue) was used as a nuclear counterstain. Left panels show stainings for the interfollicular epidermis, while the middle and right panels show stainings for hair follicles. Scale bars, 50 µm.

(b) The level of NIPP1 in extracts of tail epidermis from 4 CTRs and SKOs of 8 weeks was visualized by immunoblotting. GAPDH was used as a loading control.

(c) Quantification of the data in panel b (n = 4).

(d) qRT-PCR analysis of the *Ppp1r8* transcript in tail and back epidermis from CTRs and SKOs of 8 weeks (n=4). *Hprt* was used as a housekeeping gene for normalization.

(e) Representative pictures of the ears and tail of CTRs and SKOs at 8 weeks.

(f) Representative pictures of back skin and tail of CTRs and SKOs at 8-12 months.

(g) Ulcerated skin lesions in SKOs of 8 months.

(h) Quantification of transepidermal water loss (TEWL) from the back of CTR and SKO mice of 8 weeks (n=6).

The bar graphs are represented as means ± SD. **, $p<0.01$; ***, $p<0.001$ (unpaired student's t-test).

Figure 2. Epidermal hyperproliferation in SKOs.

(a) Hematoxylin-Eosin (H&E) staining of tail skin sections of CTR and SKO mice at the age of 8 weeks. Hematoxylin was used as a nuclear counterstain. The bar diagram shows quantification of the epidermal thickness (n=4).

(b-d) Tail skin sections from 8-week-old CTR and SKO mice were immunostained for incorporated BrdU after 4h-pulse (**b**) and for the proliferation markers Ki67 (**c**) and H3S10ph (**d**). Propidium iodide (PI) (**b**) or dapi (**c, d**) were used as nuclear counterstain. Bar diagrams

show the quantifications of the corresponding immunostainings (a, b and d, n=4; c, n=2). Scale bars, 25 µm.

(e-h) Tail skin sections from 8-week-old CTR and SKO mice were immunostained for Keratin-10 (KRT10) (**e**), Keratin-1 (KRT1) (**f**), Filaggrin (FLG) (**g**) and Loricrin (LOR) (**h**). Dapi was used as a nuclear counterstain. Bar diagrams show the quantifications of layer thickness (n=4). Scale bars, 25 µm.

(i) Tail epidermal wholemounts of 8-week-old CTR and SKO mice were immunostained for the integrin ITGA6 (green) and quantified by measuring the mean intensity (n=3). Dapi was used as a nuclear counterstain. Scale bars, 100 µm.

(j) Tail skin sections from 8-week-old CTR and SKO mice were immunostained for the integrin ITGB4 (green) and quantified (n=4). Dapi was used as a nuclear counterstain. Scale bars, 50 µm.

Bar data are represented as means ± SD. *, $p<0.05$; **, $p<0.01$; ***, $p<0.001$ (unpaired student's t-test).

Figure 3. Hyperproliferation, partial loss and reduced stemness of HFSCs in SKOs.

(a-d) Tail epidermis wholemounts of 8-week-old CTR and SKO mice were immunostained for the basal layer marker Keratin-14 (KRT14) (**a-c**), the bulge marker Keratin-15 (KRT15) (**b, c**), the sebaceous gland marker Fatty acid synthase (FASN) (**d**), and the proliferation maker Ki67 (**d**). Dapi was used as a nuclear counterstain. BF, bright field. Scale bars, 500 µm (**a, b**) and 100 µm (**c, d**). SG, sebaceous gland; IFD, infundibulum; HF, hair follicle.

(**e**) Quantification of Ki67-positive cells in telogen HFs as shown in (**d**) (bar diagram, n=3). Ki67-positive cells were counted in the total HF except for the hair germ.

(**f**) Tail skin sections from CTR and SKO mice of 10 weeks were immunostained for the bulge HFSC marker CD34 and the proliferation marker Ki67. Double-positive cells are indicated by

white arrowheads. The number of Ki67-positive, CD34-positive cells in the HF in tail skin was quantified (bar diagrams, n=4). Dapi was used as a nuclear counterstain. Scale bars, 100 µm.

(g) qRT-PCR analysis of the indicated HFSC markers in tail epidermis of CTR and SKO mice of 8 weeks (n=4). *Hprt* was used as housekeeping gene for normalization.

(h) Tail skin sections from CTR and SKO mice of 8 weeks were immunostained for the HFSC marker SOX9. The number of positive cells per HF was quantified (bar diagrams, n=4). Dapi was used for nuclear staining. Scale bars, 75 µm.

(i) Tail epidermal wholemounts from EdU-injected CTR and SKO mice were stained for EdU. White dots are EdU-positive cells (i.e. label retaining cells (LRCs)), while the white signal in the lowest part of the HF is caused by autofluorescence of the hair shaft. LRCs are indicated by white arrowheads. Dapi was used as a nuclear counterstain. Scale bars, 100 µm. Bar diagrams (n=4) show the quantification of the number of EdU-positive cells in the hair follicle (HF).

(j) qRT-PCR analysis of the indicated genes in FACs purified HFSCs (n=3). *Hprt* was used as a housekeeping gene for normalization.

Bar data are represented as means ± SD. *, $p<0.05$; **, $p<0.01$; ***, $p<0.001$ (unpaired student's t-test).

Figure 4. Sterile inflammation in the SKOs.

(a) Tail-skin sections from CTR and SKO mice of 8 weeks were immunostained for the pan-immune cell marker CD45. Dapi was used as a nuclear counterstain. Bar diagrams show the quantifications (n=4). Area = 100.000 µm². For each mouse, 15 pictures were analysed and the area was extrapolated to 100.000 µm². Scale bars, 50 µm.

(b) Flow-cytometric quantification of CD45+ cells in the tail skin of 8-week-old CTRs and SKOs (n=6).

(c) Representative flow-cytometric profiles and quantifications of the indicated types of CD45+ immune cells in the tail skin of 8-week-old CTR and SKO mice (n=6).

The bar data are represented as means ± SD. *, $p<0.05$; **, $p<0.01$ (unpaired student's t-test).

Figure 5. Contribution of chemokine-driven sterile inflammation to the SKO phenotype.

(a) Scheme for the treatment of CTRs and SKOs with vehicle (VEH) or dexamethasone (DEX). Skin samples were isolated 24h after the last treatment.

(b) Immunostaining of tail skin sections from vehicle/dexamethasone-treated CTRs and SKOs for H3S10ph. Bar diagrams show quantifications of H3S10ph immunostainings in the interfollicular epidermis (IFE; n=4). Scale bars, 75 µm.

(c, d) qRT-PCR analysis for the expression of the adherence markers *Itga6* and *Itgb1* (**c**) and the HFSC marker *Krt15* (**d**) in vehicle/dexamethasone-treated skin samples.

(e) Volcano plot of differentially expressed genes between CTR and SKO mice of 8 weeks (n=4). The triangles are colored blue and red if they are classified as down- or upregulated genes, respectively, based on the corrected *p*-values (FDR<0.01, denoted by the horizontal green-colored line) and an absolute log2-ratio larger than 1 (denoted by the vertical green-colored lines.

(f-h) Bars charts of expression data of the indicated genes (FDR<0.01). The indicated genes belong to the families of chemokines and tumor necrosis factors (**f**), extracellular matrix proteins (**g**), or antimicrobial peptides (**h**). Data are expressed as a fold change ± SD (n=4) in the SKOs as compared to CTRs. The expression of all described genes (**f-h**) is significantly different between CTRs and SKOs based on the corrected *p*-value (FDR<0.01) of the RNA-seq analysis.

The bar data in b-d are represented as means ± SD (n≥3). *, $p<0.05$; **, $p<0.01$ (unpaired student's t-test). The bar data in f-h are represented as means ± SD.

Figure 6. Chemokine release from NIPP1-depleted keratinocytes.

(a) Schematic representation of FACS purification of HFSCs and basal epidermal cells (BECs).

(b, c) qRT-PCR analysis of the expression of *Ccl1* (**b**) and *Ccl2* (**c**) in total epidermis and FACS-purified HFSCs and BECs.

(d, e) qRT-PCR analysis of the expression of *Ccl1* (**d**) and *Ccl2* (**e**) in vehicle/dexamethasone-treated mice, as described in Fig. 5a.

(f-i) qRT-PCR analysis of the expression of *Ccl1* (**f**), *Ccl2* (**g**), *S100a8* (**h**), and *Cd45* (**i**) in tail epidermis of CTR and SKOs at the indicated ages.

(j) qRT-PCR analysis of the indicated transcripts in the human keratinocyte cell line HaCaT after treatment with NIPP1-specific siRNA (NIPP1 KD) or nontargeted siRNA (Ctr KD) for 24 h.

(k) Model of chemokine-induced inflammation in the SKOs. NIPP1-null keratinocytes secrete pro-inflammatory chemokines, which attract and activate immune cells that secrete additional cytokines and thereby contribute to the inflammatory response.

For all qRT-PCR data, *Hprt* was used as a housekeeping gene for normalization. All data are represented as means ± SD ($n \geq 3$). *, $p<0.05$; **, $p<0.01$; ***, $p<0.001$ (unpaired student's t-test).

Figure 1

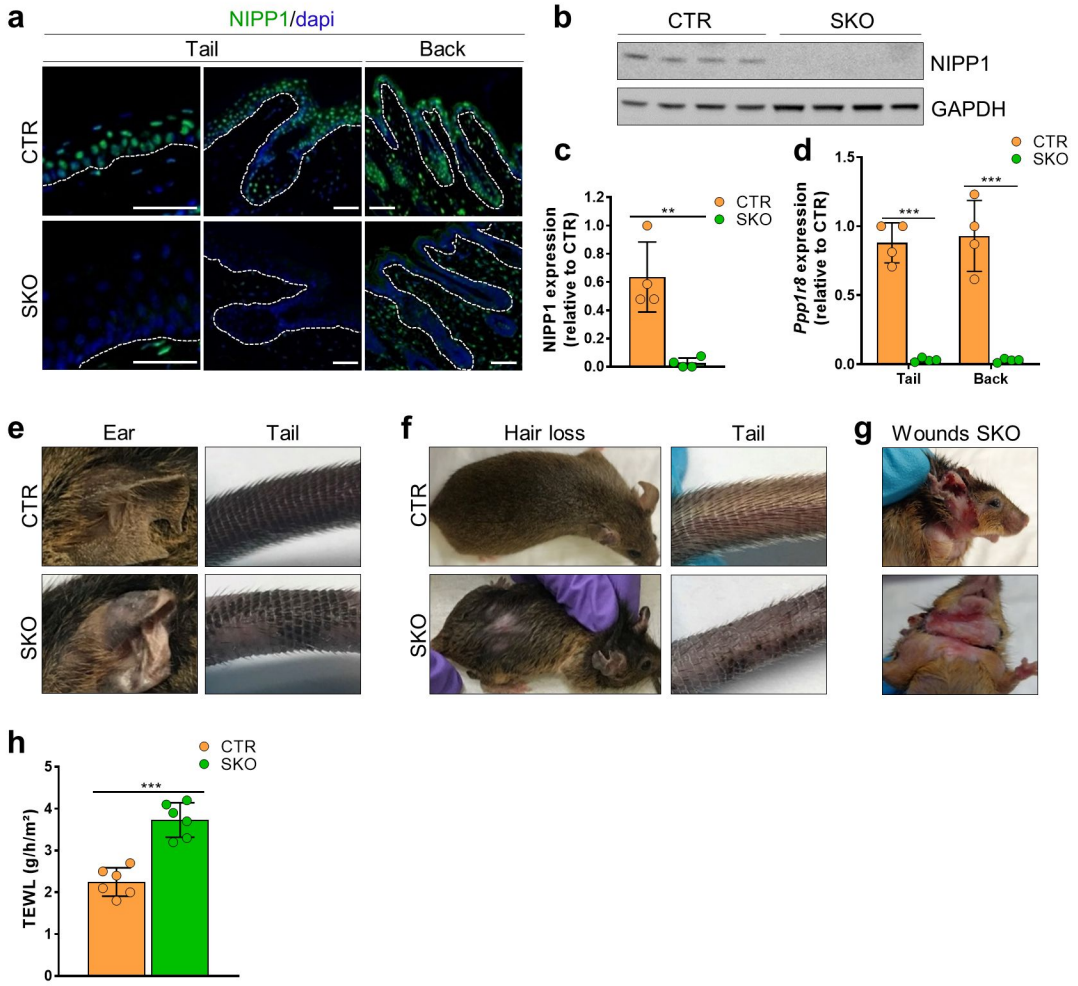
a
NIPP1/dapi
Tail
Back
CTR
SKO
b
CTR
SKO
NIPP1
GAPDH
c
NIPP1 expression (relative to CTR)
CTR
SKO
**
d
Ppp1r8 expression (relative to CTR)
CTR
SKO
***
***
Tail
Back
e
Ear
Tail
CTR
SKO
f
Hair loss
Tail
CTR
SKO
g
Wounds SKO
h
TEWL (g/h/m²)
CTR
SKO
***

Figure 2

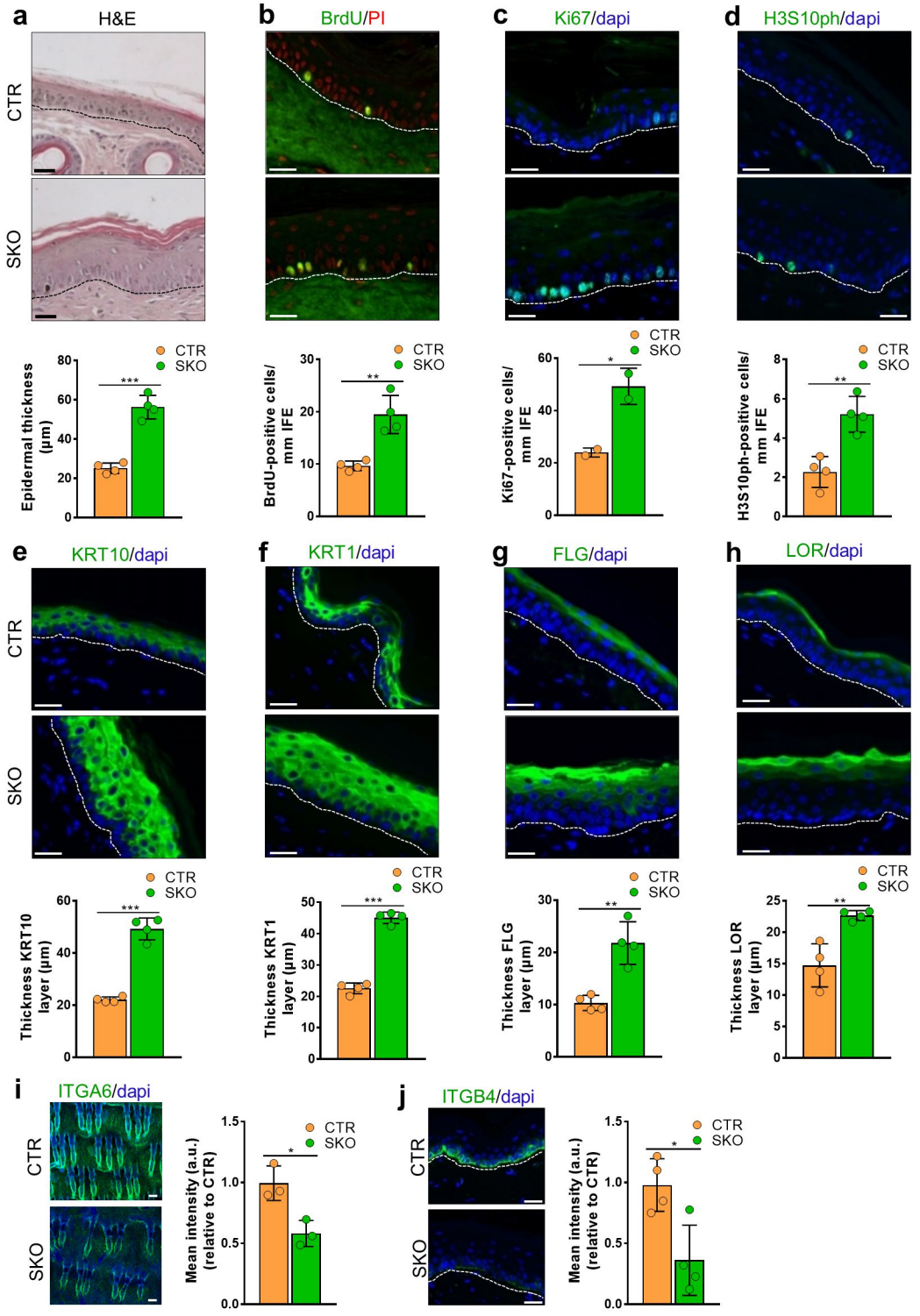
a
H&E
CTR
SKO
Epidermal thickness (µm)
b
BrdU/PI
BrdU-positive cells/ mm IFE
c
Ki67/dapi
Ki67-positive cells/ mm IFE
d
H3S10ph/dapi
H3S10ph-positive cells/ mm IFE
e
KRT10/dapi
Thickness KRT10 layer (µm)
f
KRT1/dapi
Thickness KRT1 layer (µm)
g
FLG/dapi
Thickness FLG layer (µm)
h
LOR/dapi
Thickness LOR layer (µm)
i
ITGA6/dapi
Mean intensity (a.u.) (relative to CTR)
j
ITGB4/dapi
Mean intensity (a.u.) (relative to CTR)

Figure 3

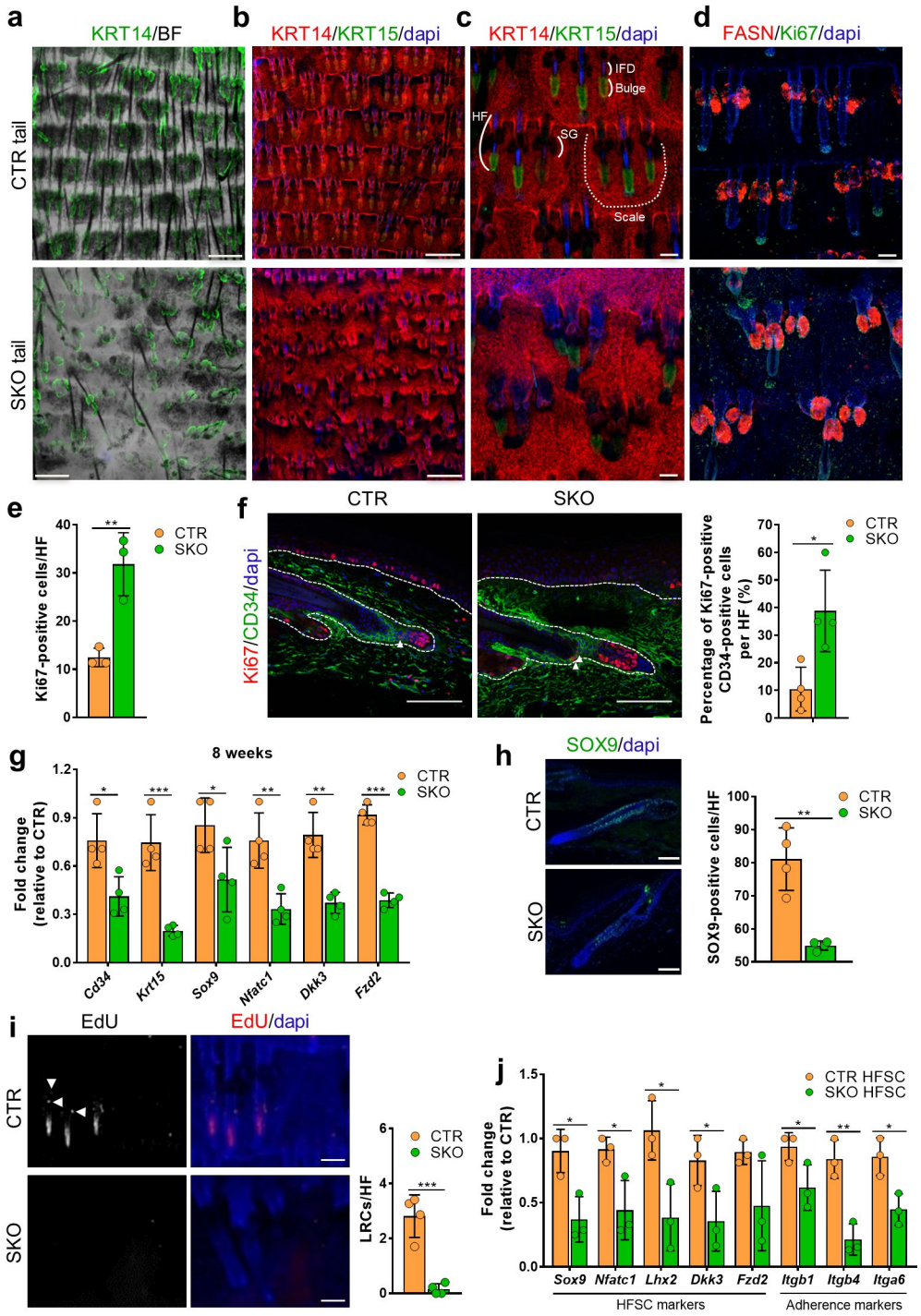
a
KRT14/BF
b
KRT14/KRT15/dapi
c
KRT14/KRT15/dapi
d
FASN/Ki67/dapi
CTR tail
SKO tail
IFD
Bulge
HF
SG
Scale
e
Ki67-positive cells/HF
CTR
SKO
f
CTR
SKO
Ki67/CD34/dapi
Percentage of Ki67-positive CD34-positive cells per HF (%)
g
8 weeks
Fold change (relative to CTR)
Cd34
Krt15
Sox9
Nfatc1
Dkk3
Fzd2
h
SOX9/dapi
SOX9-positive cells/HF
i
EdU
EdU/dapi
LRCs/HF
j
CTR HFSC
SKO HFSC
Fold change (relative to CTR)
Sox9
Nfatc1
Lhx2
Dkk3
Fzd2
Itgb1
Itgb4
Itga6
HFSC markers
Adherence markers

Figure 4

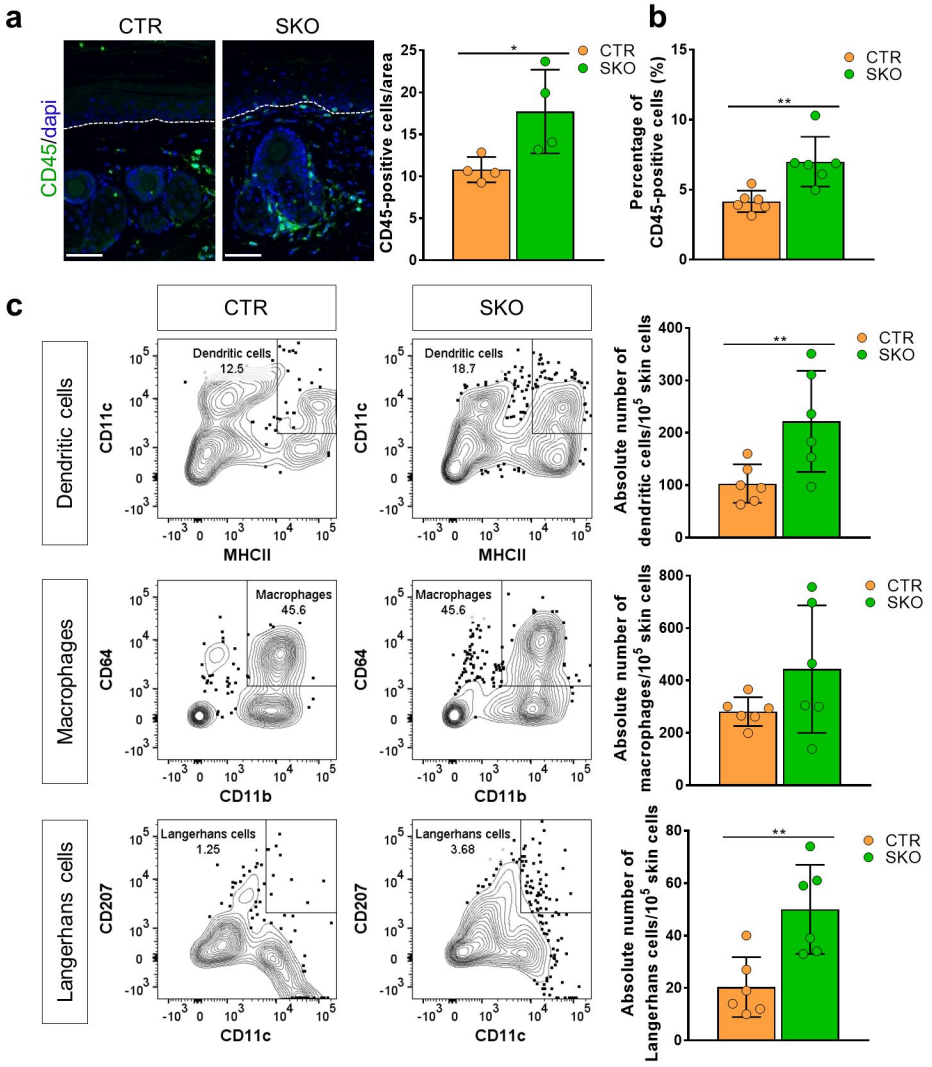
a
CTR
SKO
CD45/dapi
CD45-positive cells/area
CTR
SKO
b
Percentage of CD45-positive cells (%)
c
Dendritic cells
Macrophages
Langerhans cells
Dendritic cells 12.5
Dendritic cells 18.7
Macrophages 45.6
Langerhans cells 1.25
Langerhans cells 3.68
CD11c
MHCII
CD64
CD11b
CD207
Absolute number of dendritic cells/10^5 skin cells
Absolute number of macrophages/10^5 skin cells
Absolute number of Langerhans cells/10^5 skin cells

Figure 5

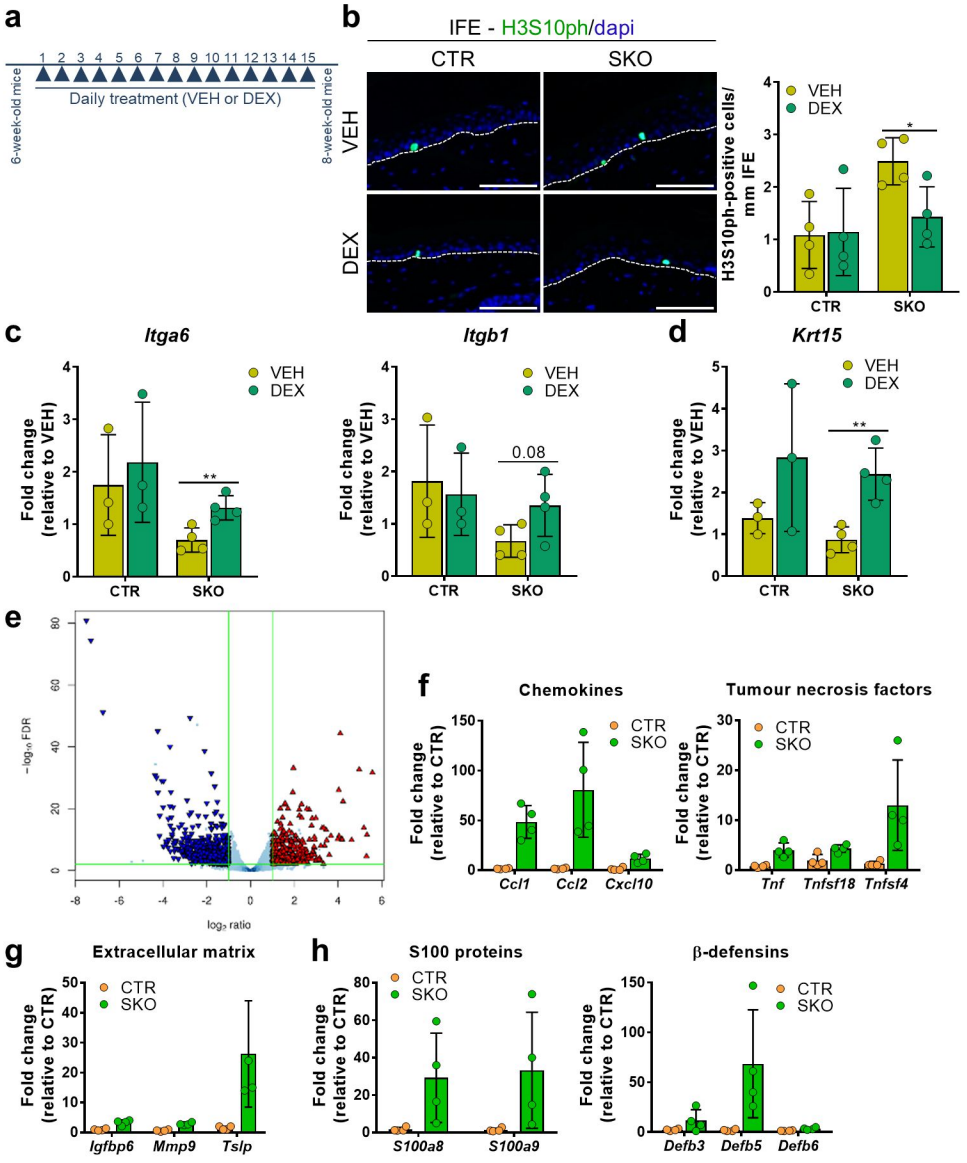
a
6-week-old mice
1 2 3 4 5 6 7 8 9 10 11 12 13 14 15
Daily treatment (VEH or DEX)
8-week-old mice
b
IFE - H3S10ph/dapi
CTR
SKO
VEH
DEX
H3S10ph-positive cells/ mm IFE
VEH
DEX
CTR
SKO
c
Itga6
Itgb1
Fold change (relative to VEH)
VEH
DEX
0.08
d
Krt15
e
−log10 FDR
log2 ratio
f
Chemokines
Tumour necrosis factors
Fold change (relative to CTR)
CTR
SKO
Ccl1
Ccl2
Cxcl10
Tnf
Tnfsf18
Tnfsf4
g
Extracellular matrix
Igfbp6
Mmp9
Tslp
h
S100 proteins
S100a8
S100a9
β-defensins
Defb3
Defb5
Defb6

Figure 6

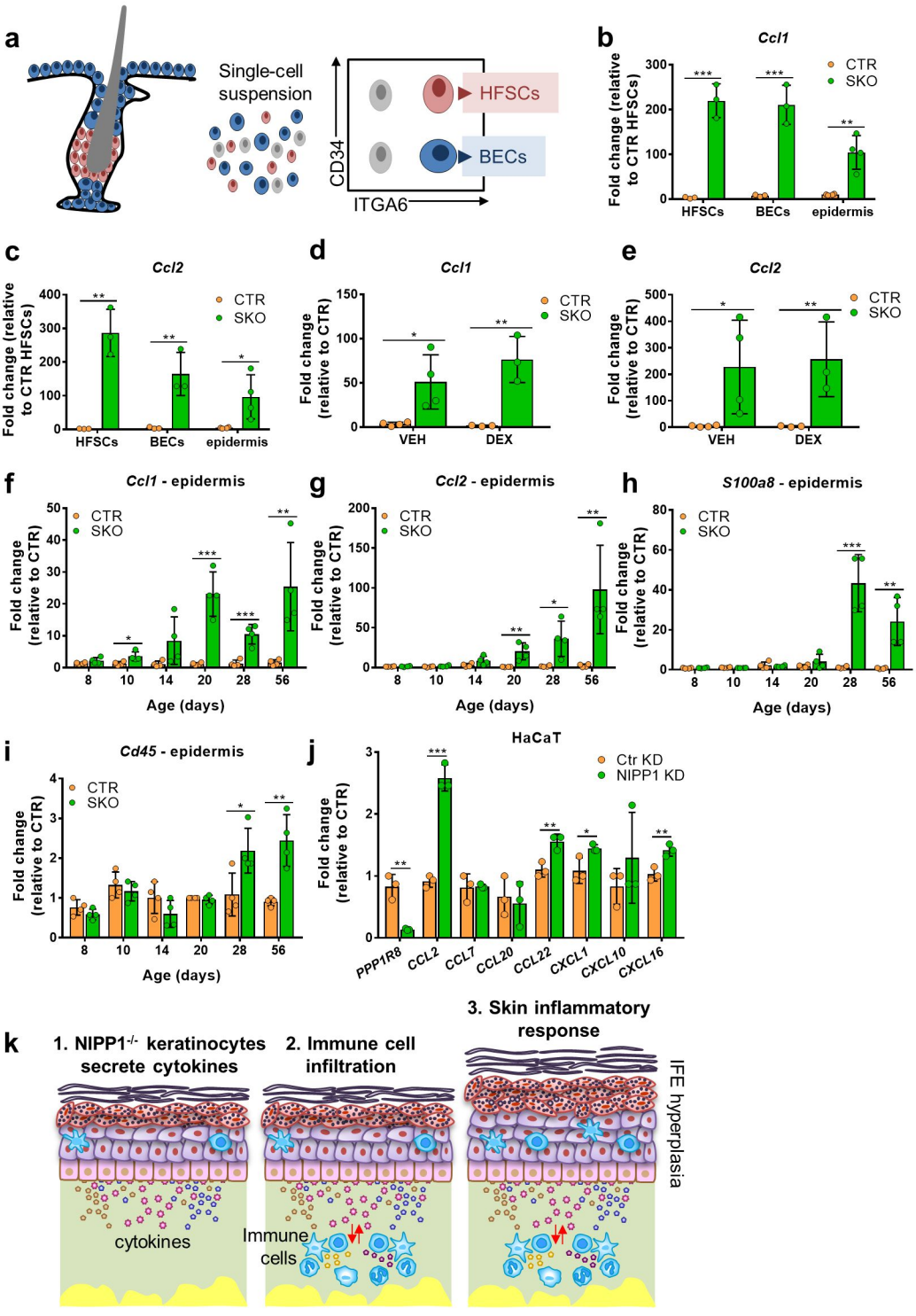
a
Single-cell suspension
HFSCs
BECs
CD34
ITGA6
b
Ccl1
Fold change (relative to CTR HFSCs)
CTR
SKO
HFSCs
BECs
epidermis
c
Ccl2
Fold change (relative to CTR HFSCs)
d
Ccl1
Fold change (relative to CTR)
VEH
DEX
e
Ccl2
f
Ccl1 - epidermis
Age (days)
g
Ccl2 - epidermis
h
S100a8 - epidermis
i
Cd45 - epidermis
j
HaCaT
Ctr KD
NIPP1 KD
PPP1R8
CCL2
CCL7
CCL20
CCL22
CXCL1
CXCL10
CXCL16
k
1. NIPP1-/- keratinocytes secrete cytokines
2. Immune cell infiltration
3. Skin inflammatory response
cytokines
Immune cells
IFE hyperplasia

The phosphatase regulator NIPP1 restrains chemokine-driven skin inflammation

Iris Verbinnen[1], Marloes Jonkhout[1], Kifayathullah Liakath-Ali[2], Kathelijne Széker[1], Mónica Ferreira[1], Shannah Boens[1], Raphael Rouget[1], Margareta Nikolic[1], Susan Schlenner[3], Aleyde Van Eynde[1], and Mathieu Bollen[1]

SUPPLEMENTARY INFORMATION

- Supplementary figures S1-S6 and supplementary legends to the figures and Movie S1.
- Supplementary Materials and Methods.
- Supplementary references.
- Supplementary table S1: primers for genotyping.
- Supplementary table S2: antibodies.
- Supplementary table S3: RT-qPCR primers.
- Supplementary table S4: Differentially expressed genes (DEGs) SKOvsCTR (FDR<0.01, two-fold cut-off).
- Supplementary table S5: Downregulated DEGs (SKOvsCTR) are enriched for *Krt* and *Krtap* genes.
- Supplementary table S6: Overlap of upregulated DEGs (SKOvsCTR) and the GO_Immune_System_Process gene set.
- Supplementary Movie S1

Figure S1

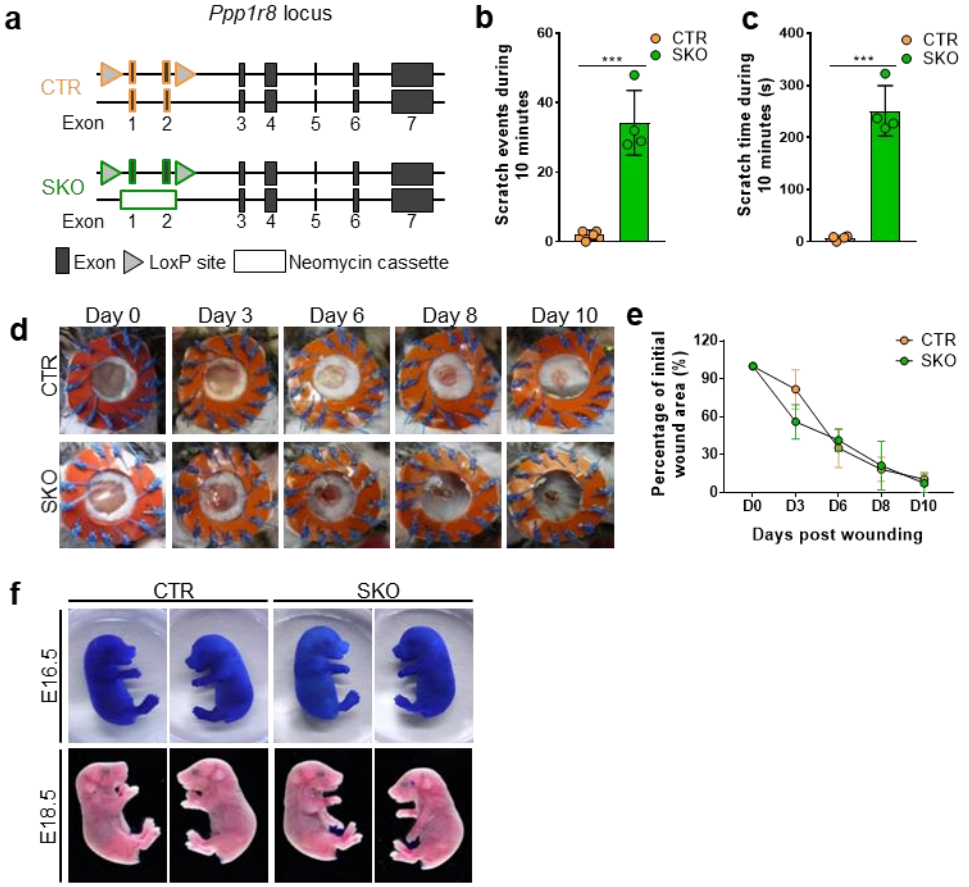

Supplementary Figure 1. Generation and phenotype of skin-specific *Ppp1r8* knockout mice.

(a) Schematic representation of the genotype of keratinocytes of CTR and SKO mice. CTR, Tg(Krt14-Cre)/*Ppp1r8*$^{fl/+}$; SKO, Tg(Krt14-Cre)/ *Ppp1r8*$^{fl/-}$. **(b)** Quantification of scratch events during 10 minutes by CTR and SKO mice of 6-7 months (n=4). **(c)** Quantification of scratch time during 10 minutes by CTR and SKO mice of 6-7 months (n=4). **(d)** Representative pictures of healing of 5-mm punch wounds in CTR and SKO back skin. **(e)** Quantification of wound healing as shown in panel d (5 CTR and 3 SKO). **(f)** Representative images of toluidine blue stainings of CTR and SKO embryos at E16.5 and E18.5.

Bar data are represented as means ± SD. ***, $p<0.001$ (unpaired student's t-test).

Figure S2

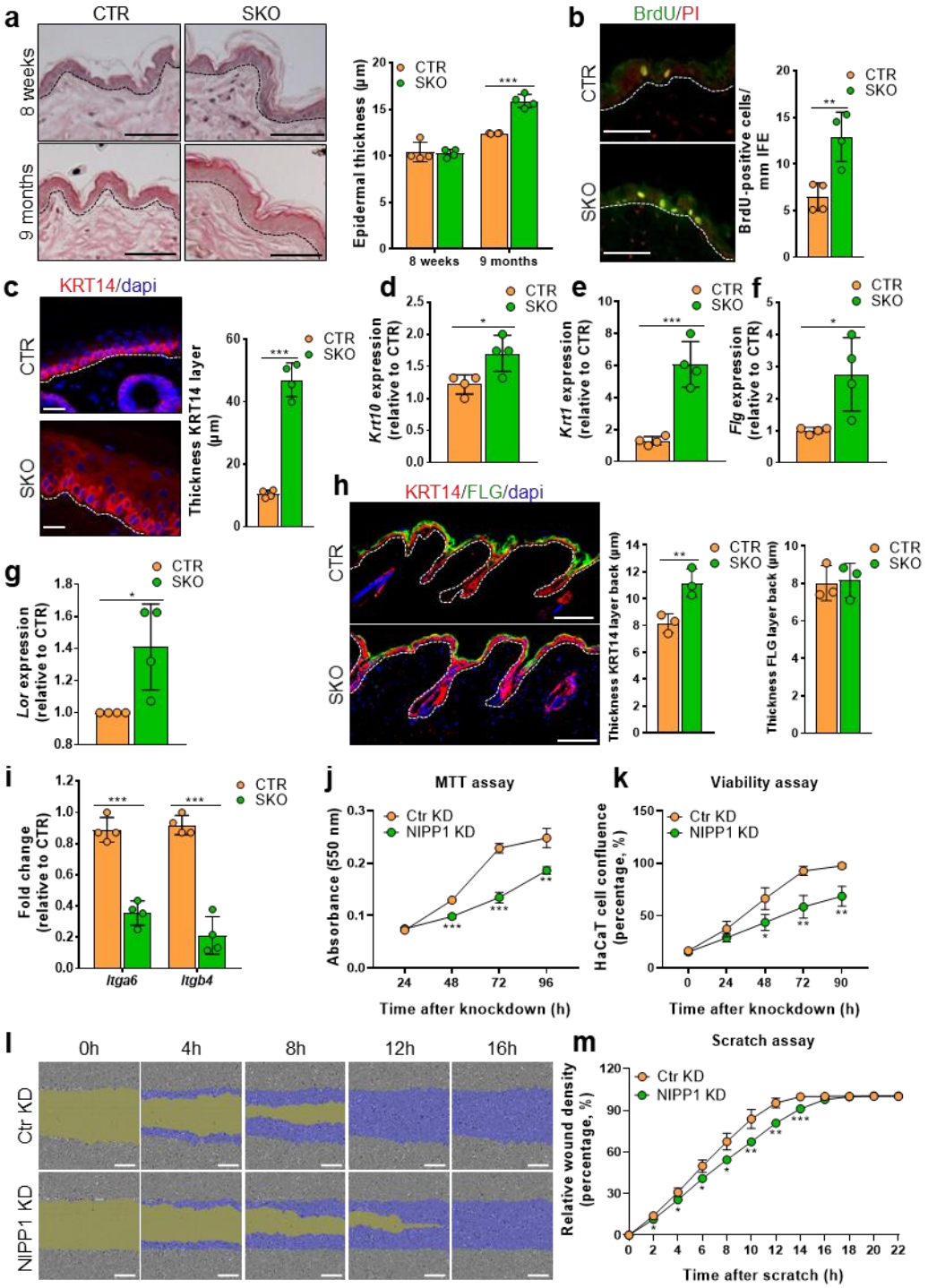

Supplementary Figure 2. Hyperproliferation phenotype in SKOs.

(a) H&E stainings of back skin sections of CTR and SKO mice at the age of 8 weeks and 9 months. Hematoxylin was used as a nuclear counterstain. Scale bars, 50 µm. The bar diagrams

show the quantification of epidermal thickness (n=4). **(b)** Back skin sections from CTRs and SKOs of 8 weeks were immunostained for incorporated BrdU after a 4h pulse labeling. Propidium iodide (PI) was used as a nuclear counterstain. The bar diagrams show the quantification (n=4). **(c)** Tail skin sections from CTRs and SKOs of 8 weeks were immunostained for Keratin-14 (KRT14). Control stainings (i.e. no primary antibody, only secondary antibody) were negative. Dapi was used as a nuclear counterstain. The bar diagram shows the quantification of layer thickness based on the KRT14 immunostainings (n=4). Scale bars, 25 µm. **(d-g)** qRT-PCR analysis of the indicated differentiation markers in tail epidermis from 8-week-old CTR and SKO mice. *Hprt* was used as housekeeping gene for normalization (n=4). **(h)** Back skin sections from CTR and SKO mice of 8 weeks were immunostained for KRT14 and Filaggrin (FLG). Dapi was used as a nuclear counterstain. The bar diagrams show the quantification of layer thickness based on the KRT14- and FLG-immunostainings (indicated in the y-axis) (n=3). Scale bars, 100 µm. **(i)** qRT-PCR of integrins *Itga6* and *Itgb4* in tail epidermis from 8-week-old CTR and SKO mice. *Hprt* was used as housekeeping gene for normalization (n=4). **(j, k)** The growth rate of HaCaT cells after control (Ctr) or NIPP1 knockdown (KD) was determined by MTT assays (**j**) and viability assays (IncuCyte) (**k**) at the indicated time points. Values (points) are represented as means ± SD (n=3). **(l)** The effect of NIPP1 on cell migration was measured by the IncuCyte scratch wound assay. Representative pictures show the initial scratch wound mask (purple) that gets infiltrated by migrated HaCaT cells (yellow scratch wound mask) at the indicated time points after scratching in control and NIPP1-depleted HaCaT cells. **(m)** Wound closure during the IncuCyte scratch wound assay is shown as the relative wound density in percentage at the indicated time points. Each point is the mean of three independent experiments ± SD (n=3).

All bar data are represented as means ± SD. *, $p<0.05$; **, $p<0.01$; ***, $p<0.001$ (unpaired student's t-test).

Figure S3

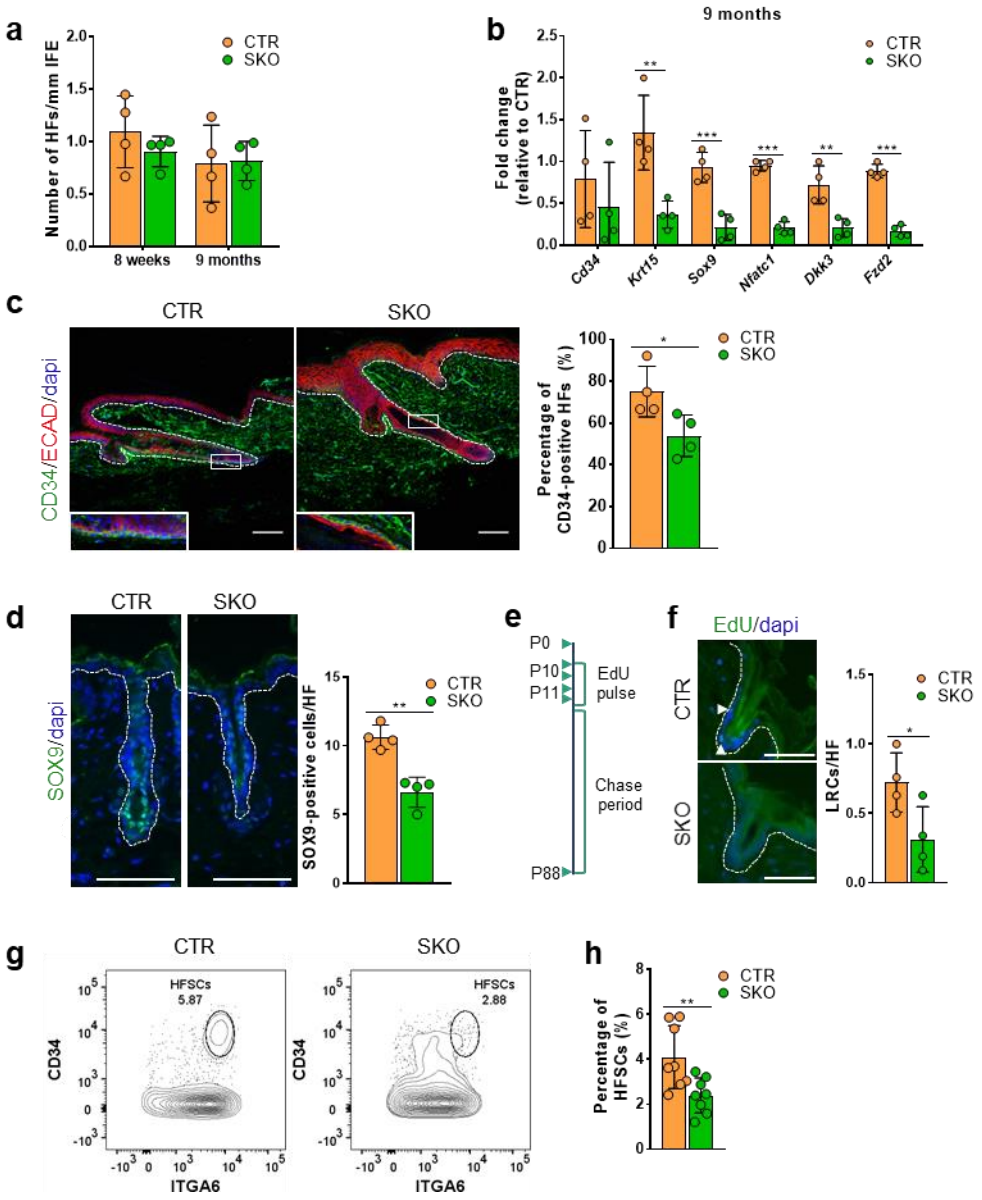

Supplementary Figure 3. The fate of HFSCs in SKOs.

(a) Quantification of the number of hair follicles (HFs) in tail skin from CTR and SKO at 8 weeks and 9 months (n=4). **(b)** qRT-PCR analysis of the indicated HFSC markers in tail epidermis from CTR and SKO mice of 9 months (n=4). *Hprt* was used as housekeeping gene for normalization. **(c)** Tail skin sections from CTR and SKO mice of 10 weeks were immunostained for the HFSC marker CD34 and the adherens junction component E-Cadherin (ECAD). The number of positive cells per HF was quantified (bar diagrams, n=4). Dapi was used for nuclear staining. Scale bars, 200 µm. **(d)** Back skin sections from CTR and SKO mice of 8 weeks were immunostained for the HFSC marker SOX9 and quantified (bar diagrams,

n=4). Dapi was used for nuclear staining. Scale bars, 75 µm. **(e)** Procedure of EdU pulse-chase experiment. 10-days-old-pups were injected intraperitoneally with 5-ethynyl-2'-deoxyuridine (EdU) every 12 hours for a total of 4 injections. Skin samples were collected 77 days after the last injection. **(f)** Back skin sections from EdU-injected CTR and SKO mice were stained for EdU. The bar diagrams show the quantification of the number of EdU-label retaining cells (LRCs) cells per hair follicle (HF). LRCs are indicated by white arrowheads. Dapi was used for nuclear staining. Scale bars, 50 µm. **(g)** Representative flow cytometry profiles of epidermal cells that were isolated from tail skin of 8-week-old CTR and SKO mice and gated for CD34 and ITGA6. **(h)** Quantification (n=8) of the frequency of HFSCs ($CD34^{high}$ $ITGA6^{high}$) by FACS sorting analysis.

Data are represented as means ± SD. *, $p<0.05$; **, $p<0.01$; ***, $p<0.001$ (unpaired student's t-test).

Figure S4

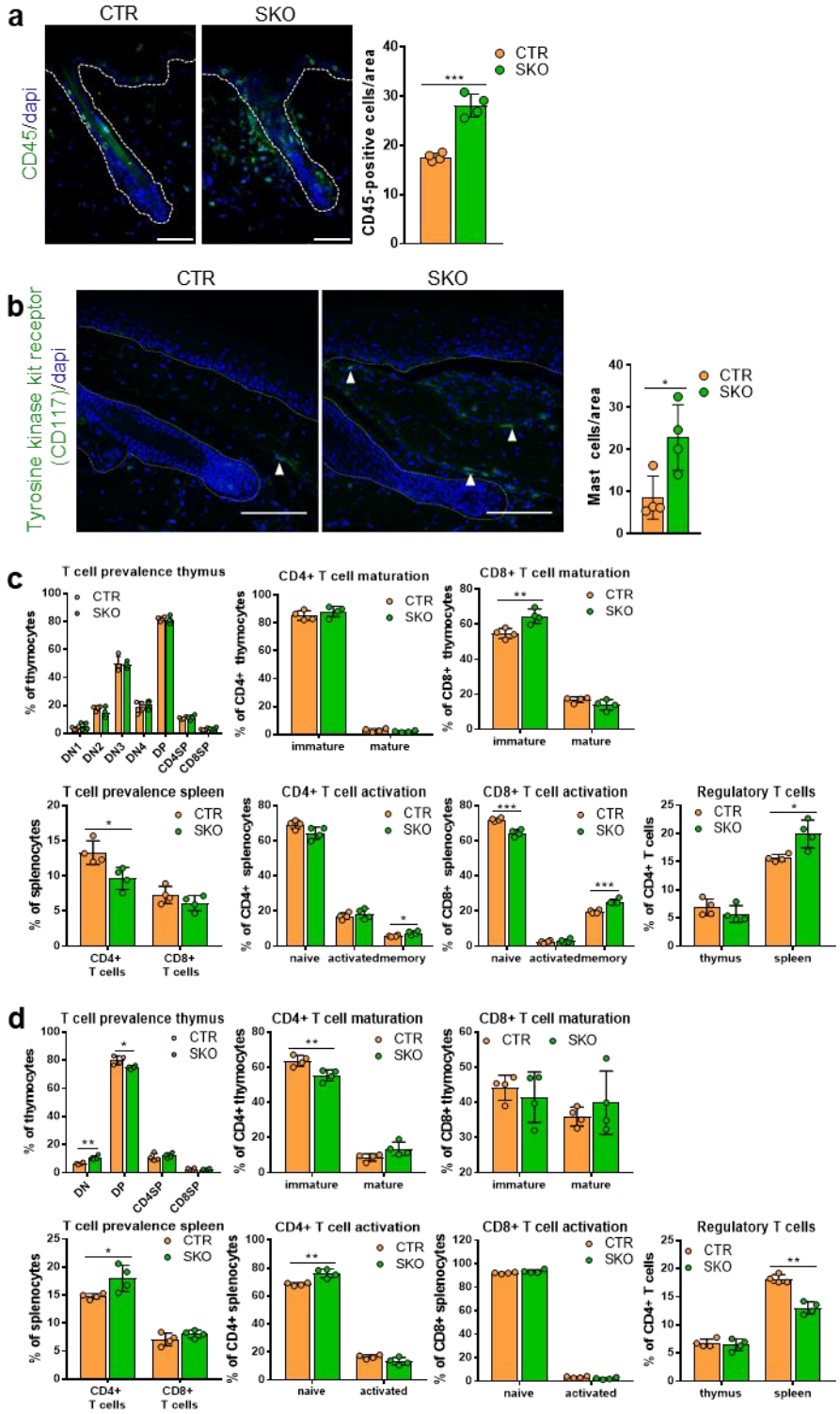
a
CTR
SKO
CD45/dapi
CD45-positive cells/area
b
Tyrosine kinase kit receptor (CD117)/dapi
Mast cells/area
c
T cell prevalence thymus
% of thymocytes
DN1
DN2
DN3
DN4
DP
CD4SP
CD8SP
CD4+ T cell maturation
% of CD4+ thymocytes
immature
mature
CD8+ T cell maturation
% of CD8+ thymocytes
T cell prevalence spleen
% of splenocytes
CD4+ T cells
CD8+ T cells
CD4+ T cell activation
% of CD4+ splenocytes
naive
activated
memory
CD8+ T cell activation
% of CD8+ splenocytes
Regulatory T cells
% of CD4+ T cells
thymus
spleen
d
T cell prevalence thymus
% of thymocytes
DN
DP
CD4SP
CD8SP
CD4+ T cell maturation
% of CD4+ thymocytes
immature
mature
CD8+ T cell maturation
% of CD8+ thymocytes
T cell prevalence spleen
% of splenocytes
CD4+ T cells
CD8+ T cells
CD4+ T cell activation
% of CD4+ splenocytes
naive
activated
CD8+ T cell activation
% of CD8+ splenocytes
Regulatory T cells
% of CD4+ T cells
thymus
spleen

Supplementary Figure 4. Immune response in SKOs.

(a) Back-skin sections from CTRs and SKOs of 8 weeks were immunostained for the pan-immune cell marker CD45. Dapi was used as a nuclear counterstain. The bar diagrams show quantifications (n=4). Scale bars, 50 µm. **(b)** Tail-skin sections from CTRs and SKOs of 10 weeks were stained for the mast-cell marker tyrosine kinase kit receptor (CD117) (left panel). Dapi was used as nuclear counterstaining. Area = 100.000 μm^2. For each mouse, 15 pictures were analyzed and the area was extrapolated to 100.000 μm^2. The bar diagrams show the quantification (n=4). Scale bars, 100 µm. **(c)** FACS analysis of T-cell prevalence in the thymus, CD4+ and CD8+ T-cell maturation, T-cell prevalence in the spleen, CD4+ and CD8+ T-cell activation and Regulatory T-cells from CTR and SKO mice of 4 weeks (n=4). **(d)** Idem as in panel (c) but for mice of 8-12 weeks (n=4).

Data are represented as means ± SD. *, $p<0.05$; **, $p<0.01$; ***, $p<0.001$ (unpaired student's t-test).

Figure S5

a

Gene set name [# genes]	# Genes in overlap	FDR
Downregulated DEGs [512] vs. GO Biological Process gene sets [4436]		
GO_Tissue_Development [1518]	53	1.01 e^{-13}
GO_Epithelium_Development [945]	38	2.27 e^{-11}
GO_Ion_Transport [1262]	44	2.27 e^{-11}
Downregulated DEGs [512] vs. GO Cellular Component gene sets [580]		
GO_Intermediate_Filament [196]	63	1.17 e^{-77}
GO_Intermediate_Filament_Cytoskeleton [239]	63	1.06 e^{-71}
GO_Supramolecular_Fiber [670]	65	9.29 e^{-45}
Downregulated DEGs [512] vs. GO Molecular Function gene sets [901]		
GO_Structural_Molecule_Activity [732]	38	3.23 e^{-15}
GO_Transmembrane_Transporter_Activity [997]	40	1.27 e^{-12}
GO_Transporter_Activity [1276]	43	2.95 e^{-11}

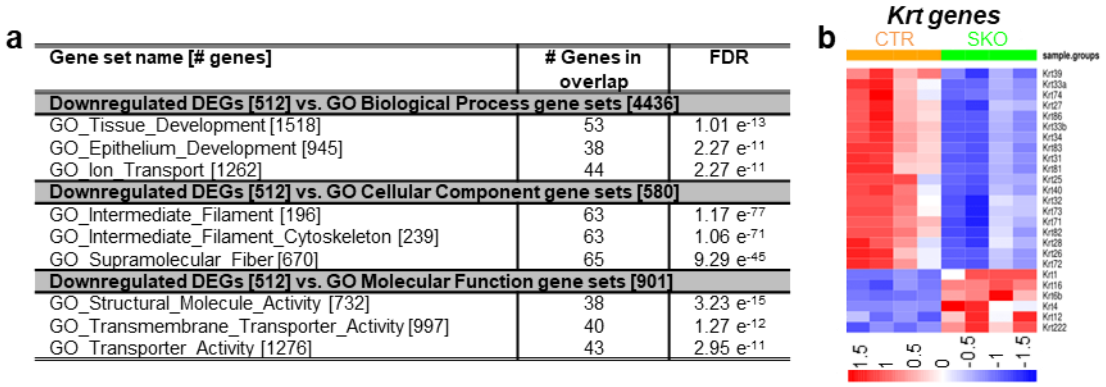

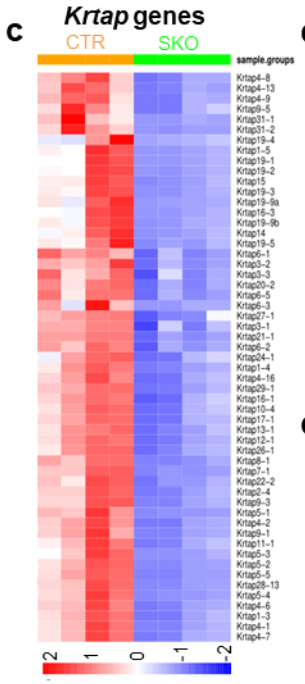

d

Gene set name [# genes]00	# Genes in overlap	FDR
Upregulated DEGs [334] vs. GO Biological Process gene sets [4436]		
GO_Immune_System_Process [1984]	90	6.68 e^{-50}
GO_Immune_Response [1100]	70	2.65 e^{-47}
GO_Defense_Response [1231]	64	1.19 e^{-37}
Upregulated DEGs [334] vs. GO Cellular Component gene sets [580]		
GO_Extracellular_Space [1376]	56	2.31 e^{-27}
GO_Intrinsic_Component_Of_Plasma_Membrane [1649]	51	1.31 e^{-19}
GO_Cell_Surface [757]	30	8.71 e^{-14}
Upregulated DEGs [334] vs. GO Molecular Function gene sets [901]		
GO_Cytokine_Activity [219]	20	4.64 e^{-15}
GO_Receptor_Binding [1476]	43	4.64 e^{-15}
GO_Protein_Complex_Binding [935]	34	1.72 e^{-14}

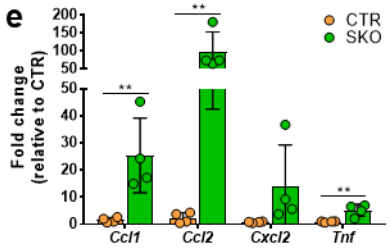

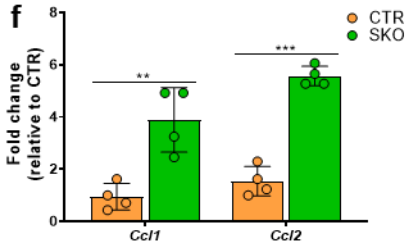

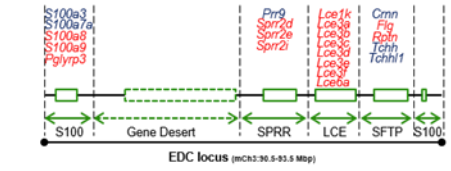

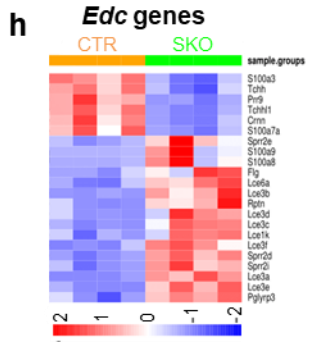

Supplementary Figure 5. Differentially expressed genes in the SKOs.

(a) Gene set enrichment analyses (GSEA) for biological, cellular and molecular function of all downregulated genes (FDR < 0.01, two-fold cut-off) in tail epidermis from CTR and SKO mice of 8 weeks. **(b-c)** Heat map of the significantly (FDR < 0.01, cut-off > 2-fold change) altered *Krt* (b) and *Krtap* (c) genes (n=4). **(d)** Gene set enrichment analyses (GSEA) for biological, cellular and molecular function of all upregulated genes (FDR < 0.01, two-fold cut-off) in tail epidermis from CTR and SKO mice of 8 weeks. **(e, f)** qRT-PCR analysis of the indicated

cytokines in tail (**e**) and back (**f**) epidermis from CTRs and SKOs of 8 weeks. *Hprt* was used as housekeeping gene for normalization. Data are represented as means ± SD (n=4). **, $p<0.01$; ***, $p<0.001$ (unpaired student's t-test). **(g)** Schematic representation of the epidermal-differentiation-complex (EDC) locus in a ~3.1 Mb region of mouse chromosome 3. This locus comprises four tandemly arrayed gene families, i.e. the calcium-binding S100 proteins, the small-proline-rich-proteins (SPRR), the late-cornified-envelope-proteins (LCE) and the S100-fused-type-proteins (SFTP). **(h)** Heat map of the significantly (FDR < 0.01, cut-off > 2-fold change) altered genes in the EDC locus (n=4).

Figure S6

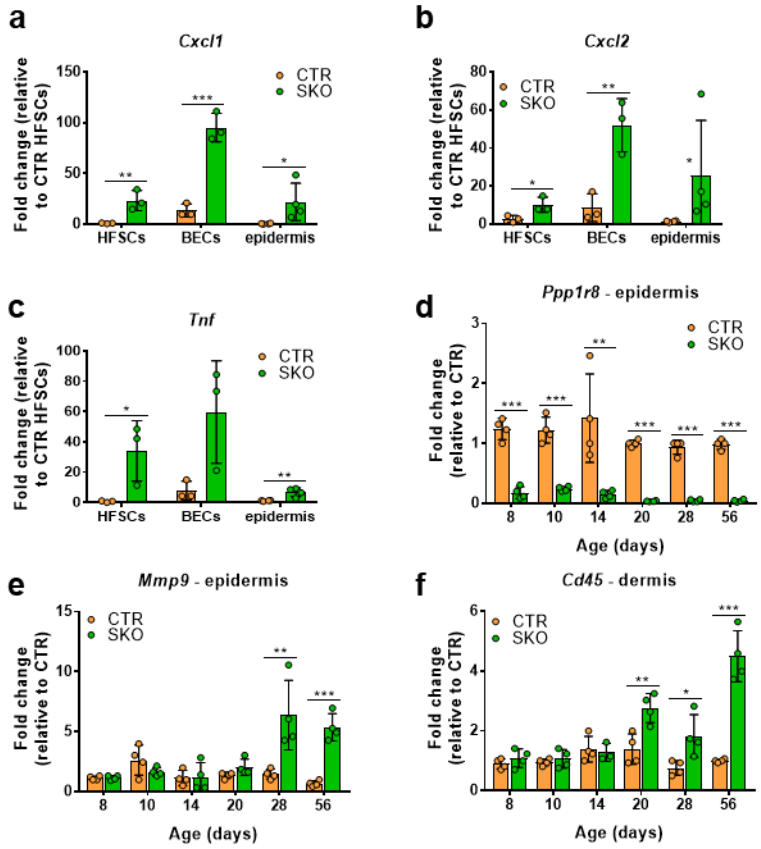

Supplementary Figure 6. Chemokine secretion in the skin of SKOs.
(a-c) qRT-PCR analysis of the indicated cytokines in FACS-purified HFSCs and BECs (n=3) and in total tail epidermis (n=4). *Hprt* was used as a housekeeping gene for normalization. **(d)** qRT-PCR analysis of *Ppp1r8* expression in tail epidermis from CTRs and SKOs of the indicated ages (n=4). *Hprt* was used as a housekeeping gene for normalization. **(e)** qRT-PCR analysis of *Mmp9* expression in tail epidermis of CTR and SKOs of the indicated ages (n=4). *Hprt* was used as a housekeeping gene for normalization. **(f)** qRT-PCR analysis of *CD45* expression in tail dermis of CTR and SKOs of the indicated ages (n=4). *Hprt* was used as a housekeeping gene for normalization.
All bar data are represented as means ± SD. *, $p<0.05$; **, $p<0.01$; ***, $p<0.001$ (unpaired student's t-test).

Supplementary Movie 1. Scratching behaviour of SKO mice.
Mice were monitored for 10 minutes with a camera and afterwards their scratching behaviour was analyzed. Movie S1 shows 20 seconds of the monitoring of two CTR (orange labels) and two SKO (green labels) mice.

SUPPLEMENTARY MATERIALS AND METHODS

Mouse treatment and experimental design

Mice were housed in a pathogen-free animal facility under standard 12h-light/dark cycles with water and chow *ad libitum*. We used CRE recombinase (CRE) under control of the *Keratin-14* (*Krt14*) promoter to disrupt *Ppp1r8* in keratinocytes from embryonic day (E) 14.5 (Vasioukhin et al. 1999). First, transgenic (Tg) *Krt14-Cre* mice (gift from Walter Birchmeier, Max-Delbrueck-Center for Molecular Medicine, Berlin, Germany) were mated with animals carrying one *Ppp1r8* null allele (*Ppp1r8*$^{+/-}$). Next, Tg*(Krt14-Cre)*/*Ppp1r8*$^{+/-}$ offspring was crossed with mice engineered to have LoxP sites in the promoter region and intron 2 of both *Ppp1r8* alleles (*Ppp1r8*$^{fl/fl}$) and described in (9). Tg*(Krt14-Cre)/Ppp1r8*$^{fl/+}$ and Tg*(Krt14-Cre)/Ppp1r8*$^{fl/-}$ were used as controls (CTR) and skin-specific NIPP1 knockout (SKO) mice, respectively (The generation of *Ppp1r8*$^{fl/fl}$ mice is described in (Boens et al. 2016). DNA used for genotyping was extracted from ear biopsies. PCR primers are described in **Table S1** and the PCR conditions are available on request. Mice were injected with 5'-bromo 2'-deoxyuridine (BrdU) (Sigma-Aldrich) 4h before they were sacrificed. Skin sections were either directly frozen in liquid nitrogen or fixed in PBS containing 4% formaldehyde, or else incubated overnight at 4°C with either 10 mg/ml dispase (Sigma-Aldrich) or 2.5 mg/ml trypsin (Sigma-Aldrich) when separation of epidermis was required. All experimental protocols were in accordance with and approved by the Guide of Care of Experimental Animals of the KU Leuven Ethical Committee (license number 053/2018).

Skin-barrier assays

For embryo whole-mount dye-penetration assays, embryos were dissected at E16.5 or E18.5, sacrificed, rinsed in PBS and quickly dehydrated and rehydrated through immersion in consecutively 25, 50, 75, 100, 75, 50 and 25% methanol, and subsequently rinsed in PBS. Staining was performed by immersion of the embryos in 0.1% toluidine blue (Fluka) in PBS

for 2 minutes. The embryos were destained in PBS at pH 7.4. The barrier function was evaluated based on the degree of dye penetration (Hardman et al. 1998). Transepidermal water loss (TEWL) was measured with the DermaLab® device (Cortex Technology). Briefly, the back skin of 8-week-old mice was shaved one day before measurements were started. TEWL measurements were always performed in the afternoon and in the same assessment room without air circulation. Room temperature (mean = 20.6°C, SD = 0.4, n=3) and humidity (mean = 62.1%, SD = 4.3; n=3) were registered before recording. For each mouse, three regions were measured in triplicate and the mean value for each region was calculated.

Assessment of scratching behaviour

Mice were monitored for 10 minutes with a camera and afterwards the number of scratch events during this time period was counted. The total scratch time during 10 minutes was also measured.

Wound-healing assay

Mice were anaesthetized with isoflurane and hair on their back skin was removed. Mice were taped on their ventral side on a heating pad. The area between the shoulders was desinfected with 2% iodine-alcohol and a piece of skin was removed with the 5-mm Stiefel biopsy punch (05.SF004.11/08). Histoacryl (Braun) was put on one side of an 8-mm silicone ring (Thermo Fisher Scientific) to tape the ring to the skin around the skin wound, and the ring was sutured to the skin using 6.0 prolene. Next, a drop of 0.9% NaCl was put in the wound to prevent it from drying out and the wound was covered with tegaderm film (Health Care). Mice were housed individually during the course of the experiment. On days 3, 6, 8 and 10 after wounding, mice were sedated with isoflurane and the tegaderm film was removed in order to take a picture of the wound. One phase exponential decay modelling in GraphPad Prism version 7 was used to compare the wound healing process between CTR and SKO mice.

EdU proliferation assay

Pups of 10 days were intraperitoneally injected with 100 µl of 6.25 mg/ml 5-ethynyl-2'-deoxyuridine (EdU) every 12 hours for a total of 4 injections and imaged using the Click-iT® EdU Alexa Fluor® 488 Imaging Kit (Thermo Fisher Scientific). Skin samples were collected 77 days after the last injection. Epidermal tail sections were prepared for wholemount staining as described previously (Liakath-Ali et al. 2014). Back skin sections were fixed in PBS containing 4% formaldehyde, embedded in paraffin and sections of 5 µm were stained. EdU detection was performed as described by the manufacturer and by Mead *et al*. 2014 (Mead and Lefebvre 2014). Microscopy was carried out using a Leica DMI 4000B microscope and images were processed with ImageJ software (National Institute of Health).

Dexamethasone treatment

Mice were intraperitoneally injected daily, for 15 consecutive days, with 4 mg/kg rapidexon/dexamethasone (Eurovet Animal Health, Dechra) or vehicle (saline). After this period, mice were sacrificed and skin tissue was used for immunohistochemical and qRT-PCR analysis.

Flow cytometry

To analyze HFSCs and BECs, flow cytometry analysis was performed as described previously (Jensen et al. 2010; Moestrup et al. 2017), with some minor modifications. Briefly, tail skin pieces were incubated overnight at 4°C with 10 mg/ml dispase (Sigma-Aldrich), and subsequently for 1h at 37°C in 2.5 mg/ml trypsin (Gibco). After separating the epidermis from the underlying dermis, single cells from the epidermis were released into suspension by breaking tissue fragments in 2.5 mg/ml trypsin (Gibco) and passing through 70-µm cell strainers (VWR international). Next, cells were counted and pelleted at 500 *g* for 8 minutes. Cells were stained with fluorescently labeled antibodies (APC-ITGA6, PE-CD34, PE/Cy7-CD45, PE/Cy7-CD31) for 1h at 0°C , washed twice with FACS buffer (PBS supplemented with 0.1% BSA) and analyzed in a BD FACSCanto II or sorted in a BD FACSAriaII (FACS core

facility, KU Leuven). Compensation was achieved by using UltraComp eBeads (Thermo Fisher Scientific). Expression of cell surface markers was analyzed on living cells after exclusion of cell doublets, CD45/CD31-positive cells and dead cells using propidium iodide (Thermo Fisher Scientific). The purity of the sorted cell populations was verified by post-sort analysis.

To analyze immune cells in the skin, flow cytometry was performed as described previously (Lay et al. 2018), with some minor adaptations. Briefly, tail skin was minced into small pieces and incubated for 75 min at 37°C in RPMI-1640 medium with L-glutamine and sodium bicarbonate (Sigma-Aldrich), supplemented with 5% FBS, 120 µg/ml Liberase TM (Roche) and 600 µg/ml DNaseI (Roche). Washing buffer containing HBSS (Gibco) and 20% FCS was added to stop the digestion. The skin pieces were squeezed through a 70-µm cell strainer (VWR international), counted and pelleted at 500 *g* for 8 minutes. Cells were stained with antibodies, including AF488-CD45, BV711-MHCII, BV605-CD11c, PE/Cy7-CD64, BUV395-CD11b, PE-CD207. Next, cells were fixed using the eBioscience Foxp3 fixation/permeabilization buffer (Thermo Fisher Scientific) and resuspended in PBS supplemented with 2.5% FCS. Dead cells were excluded by using the eF780 fixable viability dye (Thermo Fisher Scientific). Compensation was achieved by using UltraComp eBeads (Thermo Fisher Scientific). Immune cells were analysed with the BD FACSymphony A3 (FACS core facility, KU Leuven).

To analyze T cell maturation and activation by flow cytometry, thymi and spleens of 4-week-old and 8-12-week-old CTR or SKO mice were homogenized and spleens underwent red blood cell lysis. After blocking with ChromPure mouse IgG (Jackson ImmunoResearch), one half of the thymocytes were stained with CD4-PE, CD8-Fitc, CD24-PerCP-eFluor710, Qa2-biotin, Foxp3-APC and Streptavidin-BV421. Mature single positive (SP) cells were defined as CD4SP or CD8SP CD24loQa-2hi, immature SP cells were defined as CD24hiQa2lo, regulatory T-cells were identified as CD8-CD4+Foxp3+. The other half was depleted of CD8-SP cells and double positive (DP) cells using CD8-biotin and Streptavidin magnetic beads (Dynabeads

M280, Invitrogen) to enrich for double negative (DN) cells. Enriched cells were stained for Lineage-Fitc (CD4, CD11b, Gr1, CD19, CD49b, NK1.1, TCRgd, Ter119, Streptavidin-Fitc), CD25-PerCP-Cy5.5 and CD44-PE. Lineage-negative developmental stages were defined as follows: DN1 CD25-CD44+, DN2 CD25+CD44+, DN3 CD25+CD44-, CD4 CD25-CD44-. Total splenocytes were stained for CD4-Fitc, CD8-APC-Cy7, CD44-biotin/Streptavidin-BV421, CD62L-PE and Foxp3-APC. Naïve CD4 and CD8 T cells were defined as CD62L+CD44-/lo, activated CD4 and CD8 T cells as CD62L-CD44hi, and effector-memory CD4 and CD8 T cells as CD62L+CD44hi. Data of all flow cytometry experiments were analyzed using FlowJo software. The antibodies for flow cytometry are described in **Table S2**.

RNA-sequencing

Total RNA was isolated from 40 mg of snap-frozen tail epidermis from 4 CTR and 4 SKO mice (age of 8 weeks), using the GenElute^{TM} Mammalian Total RNA Miniprep kit (Sigma-aldrich). RNA integrity of the samples used for RNA sequencing was assessed using a Bioanalyser 2100 (Agilent). Library preparation, sequencing and statistical analysis of the RNA sequencing data were performed by the VIB Nucleomics Core (www.nucleomics.be), according to their standard protocols, as detailed in (Ferreira et al. 2017). All gene expression data are available at GEO under accession number GSE116844 https://www.ncbi.nlm.nih.gov/geo/query/acc.cgi?acc=GSE116844.

Histological and immunohistochemical analysis

Skin tissue was immediately fixed in PBS containing 4% formaldehyde, and embedded in paraffin at the Histology & Imaging facility (Vesalius Research Center, KU Leuven). Skin sections of 5 µm were stained with hematoxylin and eosin (H&E). For cryosections, skin tissue was fixed in PBS containing 4% formaldehyde for 20 minutes, washed twice with ammoniumchloride and incubated with 30% sucrose overnight at 4°C. The next day, the tissue was embedded in Tissue-Tek® O.C.T. Compound (Sakura). Skin sections of 10 µm were cut

with a Cryostat NX70 at the Histology & Imaging facility (Vesalius Research Center, KU Leuven). Wholemount stainings on tail skin section were prepared and performed as described previously (Liakath-Ali et al. 2014). The antibodies used for immunohistochemistry are described in **Table S2.** Microscopy was carried out using a Nikon A1R confocal, a Leica DMI 4000B, or a Leica DMBL, and images were processed with NIS Elements (Nikon Instruments) or Leica MM AF software or Leica IM50 Image Manager, respectively. Images were analyzed using ImageJ (National Institute of Health) or Icy software (Institut Pasteur, Paris, France).

Protein extraction

Epidermal lysates were made in a modified RIPA buffer containing 50 mM Tris-HCl at pH 7.5, 0.3 M NaCl, 0.5% Triton X-100, 0.2% Sodium dodecyl sulfate (SDS), 1 mM EDTA, and 0.2% sodium deoxycholate. The buffer was supplemented with protease inhibitors (1 mM phenylmethanesulfonyl fluoride, 1 mM benzamidine, 5 µM leupeptin) and protein phosphatase inhibitors (25 mM sodium fluoride, 1 mM orthovanadate). Samples were first incubated for 20 minutes on ice, and then homogenized with both a polytron blender and a Potter-Elvehjem homogenizer. Samples were incubated for 20 minutes on ice and centrifuged for 3 minutes at 11,000 *g*. The supernatant was collected and the pellet was resuspended in a buffer containing 50 mM Tris-HCl at pH 7.5, supplemented with 1.5 mM $CaCl_2$ and protease inhibitors (1 mM phenylmethanesulfonyl fluoride, 1 mM benzamidine, 5 µM leupeptin) and protein phosphatase inhibitors (25 mM sodium fluoride, 2 mM orthovanadate), and treated with 90 units of micrococcal nuclease for 30 minutes at 37°C. These lysates were centrifuged for 5 minutes at 1,700 *g* and the supernatants were retained. Both supernatant fractions were pooled and processed for SDS-PAGE and immunoblotting. Proteins were blotted on polyvinylidene fluoride membranes (GE Healthcare) and probed with various antibodies (**Table S2**). Immunoblots were visualized using ECL reagent (Perkin Elmer, Life Sciences) in the

ImageQuant LAS4000 imaging system (GE Healthcare) and were quantified using ImageQuant TL Software (GE Healthcare).

Cell culture

HaCaT cells were cultured in DMEM medium with 4.5 g/L glucose and 2 mM L-glutamine (Sigma-Aldrich), supplemented with 1 mM sodium pyruvate (Sigma-Aldrich), 10% FCS and 1% Penicillin/Streptomycin. SiRNA duplexes against human NIPP1 (stealth siRNA NIPP1, sequence: GGAACCUCACAAGCCUCAGCAAAUU) and the non-targeting control (stealth control, scrambled version of stealth siRNA NIPP1, sequence: GGAACUCGAACCUCCACGAACAAUU) were purchased from Thermo Fisher Scientific. The siRNA transfections were performed using RNAiMAX transfection reagent (Thermo Fisher Scientific). For MTT assays, 20,000 HaCaT cells were seeded in each well of a 48-well plate and knockdowns were performed as described above. 0.4 mg/ml of 3-(4,5-Dimethylthiazol-2-yl)-2,5-diphenyltetrazolium bromide (MTT) was added to each well after 24h, 48h, 72h and 96h knockdown. After 1h of incubation, the medium was removed and the purple crystals were dissolved in DMSO. The absorbance was measured at 550 nm. For viability assays, 12,000 HaCaT cells were seeded into 96-well plates and knockdowns were performed as described above. Cell confluence was automatically monitored by the IncuCyte (Essen BioScience) for 90h. For the IncuCyte scratch wound assay, HaCaT cells (60,000 cells/well) were seeded onto collagen-I-coated 96-well ImageLock tissue culture plates (Essen BioScience), knockdowns were performed as described above and the plates were incubated in a standard CO_2 incubator for 24h to form cell monolayers. Wounds were made with the 96-well WoundMaker (Essen BioScience). The wounded cells were washed twice with culture medium to remove the detached cells and then 100µl of medium was added per well. Images of the wounds were automatically acquired within the CO_2 incubator by IncuCyte zoom software (Essen BioScience). Kinetic updates were taken at 2h-intervals for 96h. The data were analysed

with respect to wound confluence and calculated by using the IncuCyte software package (Essen BioScience).

Quantitative Reverse Transcriptase (qRT) - PCR

Total RNA was isolated from snap-frozen mouse epidermis, dermis, FACS-purified BECs or from HaCaT cells (stored at -80°C) using the Genelute Mammalian Total RNA Miniprep kit (Sigma-Aldrich). Total RNA from snap-frozen FACS-purified HFSCs (stored at -80°C) was isolated using the RNeasy Plus Micro Kit (Qiagen). Complementary DNA (cDNA) was synthesized from 200 ng (minimum) and 2 µg (maximum) of total RNA using oligo (dT) primers (Sigma-Aldrich), RevertAid Premium Reverse Transcriptase and RiboLock RNase inhibitor enzymes (Fermentas). 1.2% of the cDNA was PCR-amplified in duplicate using SYBR Green qPCR Mix (Invitrogen) and a Rotorgene detection system (Corbett Research) (Boens et al. 2016). To determine the relative amount of target in different samples, all values were normalized to the housekeeping gene *Hprt* (Hypoxanthine-guanine phosphoribosyltransferase). All used qRT-PCR primers can be found in **Table S3**.

Data analysis

The results are expressed as means ± standard deviation (SD) and analyzed with the unpaired Student t-test. The wound healing process between CTR and SKO mice was compared by one phase exponential decay modelling and the difference between the fit of the curves was determined by the Mann-Whitney test. Statistical analysis was performed in GraphPad Prism version 7 (GraphPad software, Inc). All data from qPCR analysis and Western blot analysis are shown as a fold change, i.e. SKO values relative to one CTR. The value of the other CTR samples was also expressed relative to this CTR value to show the variation between the CTR samples. For the analysis of the ITGA6 and ITGB4 staining, intensity values of CTR and SKO samples were calculated with Icy. The mean value of all CTR intensity values was calculated. Next, all intensity values of CTR and SKO samples were normalized to this ‘mean CTR

intensity value'. In both wholemount sections (ITGA6) and 2D sections (ITGB4) the intensity values in IFE were quantified.

SUPPLEMENTARY REFERENCES

Boens S, Verbinnen I, Verhulst S, Szekér K, Ferreira M, Gevaert T, et al. Brief Report: The Deletion of the Phosphatase Regulator NIPP1 Causes Progenitor Cell Expansion in the Adult Liver. Stem Cells. 2016;34(8):2256–62

Ferreira M, Boens S, Winkler C, Szekér K, Verbinnen I, Van Eynde A, et al. The protein phosphatase 1 regulator NIPP1 is essential for mammalian spermatogenesis. Sci. Rep. 2017;7(1)

Hardman MJ, Sisi P, Banbury DN, Byrne C. Patterned acquisition of skin barrier function during development. Development. 1998;125(8):1541–52

Jensen KB, Driskell RR, Watt FM. Assaying proliferation and differentiation capacity of stem cells using disaggregated adult mouse epidermis. Nat. Protoc. 2010;5(5):898–911

Lay K, Yuan S, Gur-Cohen S, Miao Y, Han T, Naik S, et al. Stem cells repurpose proliferation to contain a breach in their niche barrier. Elife. 2018;7

Liakath-Ali K, Vancollie VE, Heath E, Smedley DP, Estabel J, Sunter D, et al. Novel skin phenotypes revealed by a genome-wide mouse reverse genetic screen. Nat. Commun. 2014;5

Mead TJ, Lefebvre V. Proliferation assays (BrdU and EdU) on skeletal tissue sections. Methods Mol. Biol. 2014;1130:233–43

Moestrup KS, Andersen MS, Jensen KB. Isolation and in vitro characterization of epidermal stem cells. Methods Mol. Biol. 2017. p. 67–83

Vasioukhin V, Degenstein L, Wise B, Fuchs E. The magical touch: genome targeting in

epidermal stem cells induced by tamoxifen application to mouse skin. Proc Natl Acad Sci U S A. 1999;96(15):8551–6

SUPPLEMENTARY TABLE S1: primers for genotyping.

Target	Sense Primer	Antisense Primer
K14-CRE recombinase	CTTGCGAACCTCATCACTCG	AGGGATCTGATCGGGAGTTG
NIPP1 fl/fl - Neodeletion - LoxP	CCACCCTCTCCTTTACTTTGTCTTC CTTACAAGGAGTGGTATTCGA	GGAGAGGAGTAATGAGGAGTTGTG ACTGTCTAGCAGGGCATAGTGTTG
NIPP1 knockout	CCTCAGCAGATAGCCCACGG	CGCATCGCCTTCTACGCCTTCTTGAC

SUPPLEMENTARY TABLE S2: antibodies.

Target protein	Company	Application
CD34-PE (clone RAM 34)	BD Pharmingen	FC
ITGA6-APC (clone GoH3)	Thermo Fisher Scientific	FC
CD45-PE/Cy7 (clone 30-F11)	BioLegend	FC
CD31-PE/Cy7 (clone 390)	BD Pharmingen	FC
CD45-AF488 (clone 30-F11)	BioLegend	FC
MHCII (I-A/I-E)-BV711 (clone M5/114.15.2)	BioLegend	FC
CD11c-BV605 (clone N418)	BioLegend	FC
CD64-PE/Cy7 (clone X54-5/7.1)	BioLegend	FC
CD11b-BUV395 (BD Horizon) (clone M1/70)	BD Biosciences	FC
CD207-PE (clone 4C7)	BioLegend	FC
CD4-Fitc	eBioscience	FC
CD4-PE (clone GK1.1)	eBioscience	FC
CD8-Fitc	eBioscience	FC
CD8-APC-eFluor780 (clone 53-6.7)	eBioscience	FC
CD11b (clone M2/70)	eBioscience	FC
Gr1 (clone RB6-8C5)	eBioscience	FC
CD19 (clone 1D3)	eBioscience	FC
CD49b (clone DX5)	eBioscience	FC
NK1.1 (clone PK136)	eBioscience	FC
TCRgd (clone GL3)	eBioscience	FC
Ter119 (clone Ter-119)	eBioscience	FC
Streptavidin-Fitc	eBioscience	FC
CD62L-PE (clone MEL-14)	eBioscience	FC
CD44-PE	eBioscience	FC
CD44-biotin (clone IM7)	eBioscience	FC
Foxp3-APC (clone FJK-16s)	eBioscience	FC
CD24-PerCP-eFluor710 (clone M1/69)	eBioscience	FC
CD25-PerCP-Cy5.5 (clone PC-61.5)	eBioscience	FC
Streptavidin-BV421	BioLegend	FC
Qa2-biotin (clone 1-1-2)	BD Pharmingen	FC
NIPP1	Sigma-Aldrich	IHC

Ki67 (clone SP6)	Abcam	IHC
H3S10ph (clone MC463)	Upstate Biotechnology	IHC
BrdU	Dako	IHC
Keratin-14 (clone LL002)	Abcam	IHC
Keratin-10 (clone Poly19054)	BioLegend	IHC
Keratin-1 (clone Poly19056)	BioLegend	IHC
Filaggrin	Santa Cruz Biotechnology	IHC
Loricrin (clone Poly19051)	BioLegend	IHC
Integrin-α6-FITC (clone GoH3)	BioLegend	Wholemount
Integrin-β4 (clone 346-11A)	BD Pharmingen	IHC
Directly conjugated (Alexa Fluor 555) Keratin-14 (clone LL002)	Lab Fiona Watt (King's College London)	Wholemount
Directly conjugated (Alexa Fluor 488) Keratin-15 (clone LHK-15)	Lab Fiona Watt (King's College London)	Wholemount
FASN (clone G-11)	Santa Cruz Biotechnology	Wholemount
Ki67 (NCL-Ki67p)	Novacastra	Wholemount
CD45 (clone 30-F11)	BD Biosciences	IHC
Sox9	Millipore	IHC
CD34 (clone RAM34)	Thermo Fisher Scientific	IHC
E-Cadherin (clone 24E10)	Cell Signaling Technology	IHC
CD117 (clone ACK2)	Thermo Fisher Scientific	IHC
Alexa Fluor 488 goat anti-rabbit IgG (H+L)	Invitrogen	IHC
Alexa Fluor 488 donkey anti-mouse IgG (H+L)	Invitrogen	IHC
Alexa Fluor 568 goat anti-mouse IgG (H+L)	Invitrogen	IHC
Goat anti-Rat IgG (H+L) Cross-Adsorbed Secondary Antibody, Alexa Fluor 488	Invitrogen	IHC
Goat anti-Rabbit IgG (H+L) Cross-Adsorbed Secondary Antibody, Alexa Fluor 546	Invitrogen	IHC
Swine anti-rabbit HRP	Dako	IHC + WB
Anti-mouse HRP	Dako	IHC + WB
NIPP1	Van Eynde et al. 2004	WB
GAPDH	Cell Signaling Technology	WB

FC: flow cytometry; IF: immunohistochemistry; WB: western blot

SUPPLEMENTARY TABLE S3: RT-qPCR primers.

Gene	Sense Primer	Antisense Primer
Ccl1	CCGTGTGGATACAGGATGTT	GAAGCTCTTTCTTCAAGGTGTTC
Ccl2	CTGGAGCATCCACGTGTT	GCCTACTCATTGGGATCATCTT
CCL2	TCATAGCAGCCACCTTCATTC	CTCTGCACTGAGATCTTCCTATTG
CCL20	CTCCTGGCTGCTTTGATGT	GGATGAAGAATACGGTCTGTGTAT
CCL22	GACTGCACTCCTGGTTGTC	CAGACGCTGTCTTCCATGTT
CCL7	CTCTGCAGCACTTCTGTGT	AAATCTGTAGCAGCAGGTAGTT
Cd34	ACCAGCCATCTCAGAGACTAT	GTAGTAGGCAGTATGCCAGTTG
Cd45	TGCCTATGTCAATGGGAAGATT	GGCCATTAGTTTCATAAGGAGGA
Cxcl1	TTCACCTCAAGAACATCCAGAG	AAGCCTCGCGACCATTC
CXCL1	GTGGCACTGCTGCTCCT	AGGGTCTGCAAGCACTGG
CXCL10	GCTGCCTTATCTTTCTGACTCT	GACCTTGGATTAACAGGTTGATTAC
CXCL16	CCCATGGGTTCAGGAATTGA	GGCTGGTAGGAAGTAAATGCT
Cxcl2	TCAAGAACATCCAGAGCTTGAG	CTTCAGGGTCAAGGCAAACT
Dkk3	CCAGTTCTCCAGCTTCAAGTA	CCACAGCACTCACTGTCTC
Flg	AGGAGGAAGAAACACTGAGCA	AGTTTGTCATCGTGGTCCAC
Fzd2	TGCCGTCCTATCTCAGCTATAA	CCTCTTGCGAGAAGAACATAGAG
Hprt	CTGGTGAAAAGGACCTCTCG	TGAAGTACATTATAGTCAAGGGCA
HPRT	TGACACTGGCAAAACAATGCA	GGTCCTTTTCACCAGCAAGCT
Itga6	AAGGTTTGGAGCAGATTGTTT	TTTCAGGAAGTTCCCGTTTCT
Itgb1	CAGCAACGCATATCTGGAAAC	TACATTCCTCCAGCCAATCAG
Itgb4	GGATAATACAGCACACGGACA	AGTAGCTTCACCTGCAACTC
Krt1	GACACCACAACCCGGACCCAAAACTTAG	ATACTGGGCCTTGACTTCCGAGATGATG
Krt10	GGAGGGTAAAATCAAGGAGTGGTA	TCAATCTGCAGCAGCACGTT
Krt15	GCTCAGAACCAGGAGTACAAC	AATACCAGCCATCTTAGCATC
Lor	TCACTCATCTTCCCTGGTGCTT	GTCTTTCCACAACCCACAGGA
Mmp9	CAGCCAACTATGACCAGGATAA	TCGCTGGTACAGGAAGAGTA
Nfatc1	GGCGGGAAGAAGATGGTGCTGTC	TGGTTGCGGAAAGGTGGTATCTCA
Ppp1r8	TACATCTGGATGTGGTGAAAGG	GGTCGATAGTGAAGTCACACAG

PPP1R8	TACACACGGCACTTTCTTGG	CTTGTTGTGGGCAGTGTTGA
S100a8	AAATCACCATGCCCTCTACAA	CACTATTGATGTCCAATTCTCTG AAC
Sox9	CTCTGGAGGCTGCTGAAC	CGCTTGTCCGTTCTTCAC
Tnf	TCTTCTGTCTACTGAACTTCG	GGCCATAGAACTGATGAGAG

SUPPLEMENTARY TABLE S4: Differentially expressed genes (DEGs) SKOvsCTR (FDR<0.01, two-fold cut-off).

Gene name	SKOvsCTR : logFC	SKOvsCTR : FDR
Ccl2	5.569476383	2.4143E-32
Cdkn2a	5.323965457	3.00611E-12
Stfa1	5.300138712	2.58015E-05
Defb5	5.182281401	1.72299E-14
Ccl1	4.96704325	2.31247E-33
S100a9	4.622518139	1.43652E-10
Ccl20	4.228922878	4.66147E-23
Gm5416	4.181110723	1.11493E-10
S100a8	4.174235752	5.45686E-11
Pglyrp2	4.100906903	5.13833E-45
Tslp	4.041658227	7.9062E-12
Krt6b	4.034168573	9.65337E-27
Ascl3	3.98618632	7.65471E-11
Krt4	3.675455067	6.83376E-12
Ch25h	3.599877533	9.73667E-06
Lce3b	3.480519056	1.73387E-10
Tas1r2	3.450724354	6.71019E-14
Blk	3.385207475	9.2625E-09
Lce3a	3.346668465	1.95337E-14
Gm5478	3.336928673	0.007283311
Axdnd1	3.276457843	1.82696E-14
B3gnt3	3.220092241	0.000611605
Cxcl10	3.2093752	1.16146E-08
Tnfsf4	3.157810331	8.93336E-05
Rgs4	3.124274678	0.000265427
Icos	3.025441396	0.000115095
Cxcl9	2.988683416	0.000689781
2610528A11Rik	2.985216942	1.20186E-17
Stfa2	2.940976351	1.34879E-10
Il2rg	2.924128947	5.27519E-08
5830411N06Rik	2.918900573	1.60793E-11
Ltb	2.917122347	7.03577E-06
Ccr2	2.906344841	2.25655E-08
Epb42	2.879079741	8.41099E-07
Gbp2	2.861369161	1.03382E-06
Cxcl1	2.837231096	7.51794E-07
Il18r1	2.821486218	1.32664E-17
Ccl7	2.818406405	0.000224406
Cyp7b1	2.791610531	3.23083E-15
Ppp1r1c	2.790473732	1.1543E-05
Cd247	2.7702066	6.69687E-06
Lce3e	2.694939684	9.33271E-11

Slit1	2.67632118	1.90976E-20
Rac2	2.667771175	0.000117646
Igsf6	2.640476991	1.96569E-05
Usp18	2.629431714	0.005030302
Cd3e	2.608574217	1.26872E-05
Ctsk	2.583007451	0.00012796
Slc38a5	2.57975073	0.001614665
Stfa3	2.57083166	1.959E-06
Gja4	2.569933305	1.40419E-20
Uba7	2.550012073	2.18727E-07
Lrrc9	2.528480774	1.19267E-06
Ambp	2.485060346	1.85096E-07
Defb3	2.441766769	0.002668362
Lce3f	2.440722527	1.4021E-09
Il18rap	2.43188571	6.72608E-06
Lce3d	2.388781333	1.12703E-05
Scimp	2.386576715	8.88112E-05
Ttc34	2.382470284	4.74269E-07
Pkd2l1	2.372923628	1.50725E-10
Lrrn4cl	2.369208318	5.06046E-08
Tnf	2.364621827	2.13605E-06
Adgrg3	2.341667611	1.02947E-17
Slc16a3	2.331840536	3.83735E-22
Sash3	2.310013073	0.000365201
Pmaip1	2.270588654	7.92366E-09
Ankk1	2.259416444	6.43301E-06
Fxyd1	2.259224343	0.002112139
Tmem132b	2.246987296	2.49969E-07
1700012P22Rik	2.235049877	1.66028E-18
Lax1	2.231451207	2.10887E-20
Mmp9	2.21669885	2.68206E-10
Sult4a1	2.189872386	1.44229E-06
Slc2a6	2.163465871	5.59804E-05
Pld4	2.142267156	0.000216944
Lpo	2.129146636	0.000473135
Pik3r5	2.123616919	9.82959E-05
Guca2b	2.116846777	2.82447E-08
Lcn2	2.114326884	3.1714E-10
Mfrp	2.107802037	1.74864E-05
Hgfac	2.071972951	0.008151816
Slpi	2.062517659	5.56526E-12
Gm9905	2.039170455	1.05286E-10
Ankmy1	2.037680573	2.28595E-07
Casp4	2.037305091	0.000272302

Artn	2.033294683	2.40136E-07
Casp12	2.031322192	0.002545135
Mx1	1.989569898	9.55259E-05
Apol8	1.986408619	1.3239E-08
Rgs18	1.980949482	1.26271E-05
Prl2c5	1.971858905	0.001020909
Zfp423	1.970191747	0.000683254
Ecscr	1.962364308	0.000623455
Cyp17a1	1.961045691	7.08457E-34
Sp8	1.960386478	4.17535E-06
Sprr2e	1.940237644	6.43301E-06
Chga	1.940190275	3.60766E-09
Gpr35	1.932102412	4.93457E-26
Spink14	1.914599782	7.27657E-05
Arl9	1.89873438	0.001470661
Chil1	1.892729004	9.6825E-13
Vsnl1	1.886332444	6.53537E-06
Dlgap1	1.879269433	1.76319E-10
0610009L18Rik	1.87490405	4.73939E-10
Lif	1.870071066	4.10946E-07
Il7r	1.867356535	1.58689E-08
Scd3	1.851224436	1.01996E-10
Iyd	1.837991722	0.000664947
Phf11d	1.82046899	0.000498488
Gstm6	1.818233335	4.13413E-07
Serpinb6e	1.814838497	0.006523674
Fetub	1.810969395	9.01899E-16
Igfbp6	1.809873893	7.83983E-09
Cxcr6	1.801272371	1.44983E-05
Rptn	1.793000091	2.61795E-07
Lce3c	1.766498022	1.81088E-13
C1qtnf1	1.737118642	2.49969E-07
Dnmt3l	1.733529328	0.007214623
Prr22	1.732985188	5.40831E-05
Gsta4	1.721945611	0.000788107
Dock2	1.719123784	0.000113138
Nlrc5	1.710007555	9.31974E-21
Serpina3j	1.682516956	0.005880725
Gm9958	1.663378954	2.89553E-11
Fam105a	1.644134291	2.44031E-12
Igtp	1.643225564	1.33129E-07
Tekt2	1.637897071	3.19803E-10
Tnnt2	1.633166878	1.06004E-07
Cd52	1.626022278	4.91084E-06

Avil	1.607453913	1.76872E-06
Tmem116	1.606229948	2.65307E-06
Sprr2d	1.581103301	1.87372E-22
Pla2r1	1.573835774	3.38585E-08
Acp1	1.557569955	0.000261235
Gbp7	1.555388084	7.57036E-05
Tmprss11d	1.554846328	0.002565131
Rhoc	1.549877124	4.9658E-08
Ccdc88b	1.546309694	2.7261E-05
Fgr	1.543307444	0.002954787
Krt1	1.540248096	0.000161752
Hsd11b1	1.539121421	0.003728367
Rltpr	1.536677471	0.001873894
Tnfaip2	1.534797859	6.41706E-22
Ppp2r2c	1.531602156	0.001809933
Asb2	1.525632733	9.73362E-07
Ets1	1.524817188	2.04355E-13
Ccr1	1.514548667	0.001077273
P2ry10	1.51091329	0.002136684
Psmb9	1.507861764	5.86659E-07
Casp1	1.507006458	5.48495E-07
Atp6v1g2	1.502597153	3.3679E-06
Slco2b1	1.490041713	0.003241821
Oas1e	1.489985095	0.002856819
Gbp2b	1.485426612	0.003522974
Lix1l	1.484545872	6.3643E-08
Vcam1	1.481892988	0.000570118
Itgb7	1.477629277	0.000424397
Krt16	1.473964756	4.92006E-11
Psmb8	1.468655102	4.8278E-13
Usp35	1.466275909	2.43113E-05
Lppr2	1.463648215	7.46973E-18
Gm12942	1.463444105	6.47991E-08
Tmprss11b	1.459772285	0.001052143
Fcgr2b	1.459207252	0.000407716
Hsp90ab1	1.458004795	3.07521E-09
Akt3	1.451704949	0.000226061
Rinl	1.450509541	0.000528965
Ptger1	1.448562437	7.0429E-06
Lrrc32	1.448338914	3.57313E-06
Il1f6	1.447659593	3.27643E-10
A630023A22Rik	1.445492727	2.58015E-05
Adamts5	1.445301362	2.32845E-12
Parp14	1.4446802	2.12056E-10

4930524J08Rik	1.444065121	0.000905329
Fst	1.442738865	2.5538E-14
Krt12	1.441955562	0.005059335
Kcnip2	1.435748087	0.000600696
Tnfrsf23	1.431273359	2.44954E-10
Tas1r3	1.424785092	0.008886589
Notch4	1.421053645	0.000154891
Rp1l1	1.416874084	0.001606712
Elovl6	1.404519588	0.000901933
Ano7	1.395070174	4.01417E-06
BC100530	1.38835095	1.51921E-06
Far2	1.383858746	0.002195101
B2m	1.379895788	9.01899E-16
Slc7a3	1.379284788	0.005276774
Coro1a	1.378541738	4.59076E-06
1190005I06Rik	1.372988758	0.006396701
Enho	1.371719648	0.000477978
Defb6	1.371479895	3.58449E-07
Stab1	1.371439591	1.55919E-11
Zmat1	1.370486036	0.002338956
Dok3	1.366888127	0.000102213
Sprr2i	1.361525327	1.89933E-11
Klf2	1.36067873	0.000463746
Ptges	1.360132801	9.31974E-21
Hist2h3c2	1.35990535	0.000698934
Vim	1.353953652	4.24932E-14
Mgarp	1.352088069	2.51841E-06
Dlg4	1.3517709	0.001154768
Irgm2	1.342003782	7.74323E-05
Tdrd5	1.332225688	4.05864E-05
Fmnl1	1.32454261	7.65839E-05
Cidec	1.323611973	0.002388529
Gsdmd	1.318862445	0.000324693
Tmigd1	1.31691345	0.000196605
Lce1k	1.314200611	3.06696E-06
Agap2	1.306816594	1.94059E-09
Eda2r	1.304064289	1.58951E-10
Serpinb3a	1.290171397	5.71963E-09
Tmem240	1.288276346	0.006223369
Tbkbp1	1.286445136	6.95766E-05
Ctss	1.281983114	2.32335E-05
Kremen2	1.279217838	8.88012E-10
H2-M2	1.274909293	0.000193521
Serpinb1a	1.274715146	3.19516E-10

Zmynd15	1.272161815	0.000172857
Plod1	1.266502641	3.19516E-10
Fgfbp3	1.261790006	1.8243E-10
Cdhr1	1.261524428	0.001208473
C1rl	1.253907743	1.23164E-05
Rnf224	1.236063447	8.93336E-05
Rbp1	1.235442685	1.45781E-16
Kcnab2	1.232263077	0.001323203
Isg15	1.229937075	0.004799382
Rasl10a	1.213770978	6.42124E-05
Gm38119	1.211897505	0.00045725
Hap1	1.211340561	2.70921E-10
Lag3	1.209502858	0.000265427
Fam174b	1.209458227	0.001706874
4921536K21Rik	1.203229802	1.2284E-05
Oat	1.202028834	1.7847E-09
Lsp1	1.199125032	5.43558E-05
Pkdcc	1.196854035	0.000153731
Lrrc29	1.195152632	9.14962E-05
Agbl3	1.193393243	1.14119E-09
Col8a1	1.190208581	7.18382E-08
Icam5	1.188538385	6.76581E-07
Ly75	1.184912412	2.30916E-05
Tmem176a	1.181593968	6.8321E-10
Fas	1.177586048	0.001065651
Cyba	1.175404835	0.000487845
Tmem151a	1.174989274	9.02369E-07
Gjd3	1.174814453	0.002533001
Tnfsf18	1.173972425	0.002649254
Lat	1.169941928	0.006626504
Itgax	1.162489042	0.000340789
Dnhd1	1.154358672	0.000143204
Irf1	1.152309193	1.33336E-06
Rbp2	1.152174581	2.29358E-12
Wscd2	1.152106466	0.000601576
Tubal3	1.152102527	0.007562943
H2-Q4	1.148702009	4.43852E-05
Krt222	1.147184889	0.002381843
Anxa3	1.14686161	3.09785E-06
Tmem80	1.144960106	1.67381E-10
Lce6a	1.142422658	5.39448E-09
Kif26b	1.140830931	5.25865E-05
Selplg	1.139932891	3.85628E-05
Cd53	1.136208449	0.002822472

H2-T22	1.132000219	6.15817E-09
Spn	1.1251528	0.000638154
Lgals9	1.12183177	6.86959E-09
Tgfbr3l	1.120942178	0.00017857
Noxo1	1.118016648	2.22977E-06
Tle6	1.115395284	0.000448329
Lcp1	1.114584033	6.20328E-05
Tnfrsf25	1.114468972	0.000434425
Csf1	1.113633752	0.000200065
Itgae	1.109711816	0.003668098
Wfdc12	1.109679881	0.000367873
Elk3	1.103979318	2.84755E-06
Ybey	1.099768919	4.20173E-10
Nckap1l	1.09836085	0.000861462
Ggact	1.095909674	0.000226443
Serpinb12	1.095479028	3.29726E-06
Maneal	1.094458253	0.00398627
Hmha1	1.092803539	0.000263141
Pbx3	1.088727098	2.89623E-08
Cxcl16	1.083921222	7.89148E-10
Clec11a	1.078521113	1.01325E-05
Gm5689	1.077018704	4.8278E-13
Apobr	1.076959809	4.87173E-05
9030617O03Rik	1.076862882	0.001796449
Casq2	1.070288215	0.000536692
Zfp872	1.067888917	0.009962039
Tmem173	1.0677548	0.004052918
Kng2	1.066030109	0.000594842
Atf3	1.065355351	0.009821672
Pctp	1.064584067	1.11183E-09
Morn2	1.064103185	8.44486E-05
Tspan4	1.061875191	0.00031329
Tap2	1.061812691	5.34864E-10
Cep135	1.061449275	0.000408513
Flywch2	1.058722018	6.52811E-05
Aoc2	1.058253602	9.75131E-08
Fam162a	1.049821318	1.05134E-12
Ina	1.047481216	0.004000379
Gpm6b	1.046979905	0.005218922
3110062M04Rik	1.046039527	2.27416E-07
Mlkl	1.045480417	4.57792E-05
Upk1a	1.04403007	0.003825764
H2-Eb1	1.042248308	8.26218E-07
Itpka	1.040967333	0.004343132

Pglyrp3	1.040281782	0.000108119
Jak3	1.039237981	0.000487845
Sh2d5	1.036310468	0.002288553
Rbp7	1.031347501	1.23595E-07
Il1f5	1.031253951	1.08214E-07
Ldhb	1.031211386	1.21378E-09
Icam1	1.030354606	2.55228E-07
Bfsp1	1.030188656	3.40426E-06
C1qtnf6	1.029514441	0.004174722
Cyp3a13	1.028162535	4.34199E-07
Serpinb9	1.027089861	0.008812934
Arhgap30	1.025207634	9.08558E-06
Ppp1r14a	1.02351259	0.005156381
Zbtb48	1.022350347	1.11701E-10
Neurl1b	1.0194539	1.80078E-06
Col5a3	1.017807047	0.008812934
Flg	1.017633188	0.00035916
Acot5	1.017221714	1.35944E-05
Azin2	1.017003666	1.13486E-09
Tdrp	1.015613162	0.000644766
Acoxl	1.014305397	1.5101E-07
Tcaf2	1.012324303	3.09135E-07
Nsun5	1.010925087	2.2682E-12
Angptl4	1.010625871	0.000331721
Apoc1	1.007769351	6.86959E-09
Il33	1.004278997	0.000204035
Fhl3	1.003737961	1.21185E-05
Ccl22	1.001835942	4.66887E-06
Iqgap2	-1.004060618	0.005897679
Lap3	-1.005748064	8.85028E-08
Parp1	-1.007267422	2.09971E-11
Rnaset2a	-1.010531743	0.000507785
Vtcn1	-1.010764613	0.003723577
Gmpr	-1.011791608	0.009497407
Foxn1	-1.012345637	5.77868E-08
Sp6	-1.013668816	5.39448E-09
Dmpk	-1.014517811	5.69197E-08
Isoc2a	-1.017781609	3.88153E-06
Fstl1	-1.017867526	1.2988E-07
Rgl1	-1.02181208	3.62964E-05
Lyrm9	-1.021987568	8.73857E-06
Zdhhc15	-1.022326374	0.000157543
Mroh1	-1.024312927	5.59065E-10
Zfp786	-1.024927449	0.006934553

Ache	-1.026742114	9.76463E-06
Mical1	-1.027484337	3.48986E-11
Morn4	-1.027702553	0.001117848
Prickle1	-1.030264731	6.29E-07
Whrn	-1.032762693	2.07863E-06
Ngfr	-1.034502338	0.000751925
Tbc1d16	-1.037722838	9.50023E-08
Slc16a5	-1.038600973	0.00013107
Paqr8	-1.040364822	0.003202655
Tmem117	-1.041850602	1.90635E-05
Adamts9	-1.042237035	0.001077273
Zdhhc12	-1.042948063	0.001002224
Tspan13	-1.043015892	0.008573087
Dlx3	-1.047392892	2.13605E-06
Slc9a3r2	-1.047738199	0.008834333
Gm973	-1.050402199	4.29689E-05
Bmper	-1.051225039	0.002659409
Prkcq	-1.054019871	0.000374943
Skint10	-1.056902972	7.90313E-09
Papln	-1.058177477	0.000167712
Dapk1	-1.059848968	3.43148E-07
Npas2	-1.061383182	0.000119311
5330417C22Rik	-1.065529443	0.005733133
Foxq1	-1.066666888	3.18318E-10
Car6	-1.06750232	0.000274452
Gna14	-1.068097494	1.63321E-05
E2f7	-1.069761038	0.000136897
Pitpnc1	-1.074713002	7.55963E-08
Lgals3bp	-1.084948558	0.000136897
Rab44	-1.086003205	0.001922212
Otop2	-1.093862057	0.002129197
Kcng4	-1.095442812	0.002399151
Ccdc171	-1.100997152	0.001685961
Tmem45a2	-1.102796862	7.54719E-06
Cecr2	-1.105080225	8.34106E-05
Sptb	-1.109889144	0.003104057
Ptpru	-1.110851465	1.21424E-05
Cadm4	-1.110906206	3.02598E-05
C130074G19Rik	-1.113017456	0.007584093
Slc43a1	-1.113809261	1.01274E-06
Fn1	-1.115696191	7.65871E-06
Tet1	-1.11677107	0.004785037
Sema7a	-1.120747673	1.57182E-07
Kcnn1	-1.125586145	0.001470661

Rbms3	-1.137925579	0.000156467
Cntfr	-1.141216183	0.000144901
Cdc42ep2	-1.141281203	0.002659263
Cpxm1	-1.141510509	0.000167937
Slc6a4	-1.142958641	4.37242E-12
Grik5	-1.145901676	0.000145842
Cyp2f2	-1.146137445	0.004119352
Rnf128	-1.147628494	0.000237162
Man1c1	-1.150844194	7.74898E-05
Bmp4	-1.156001429	7.03476E-05
Tnfrsf22	-1.157687569	0.000752728
Selenbp1	-1.159781968	3.16434E-12
Dlx1	-1.159928056	2.7261E-05
Tnik	-1.165670792	5.28645E-05
Tmod2	-1.165974309	0.007701554
Srl	-1.166566047	2.74923E-07
Hoxc13	-1.167893215	4.45346E-09
Grem1	-1.168917857	0.002198622
Rasl11b	-1.171176609	0.001298316
Ggt1	-1.171327471	0.005978384
Rhpn2	-1.175231992	4.83181E-05
Nrcam	-1.17631259	0.000269588
Sox6	-1.179194372	7.08337E-08
Pls1	-1.180880281	0.003745835
Phactr1	-1.181982229	0.000639776
Rerg	-1.183179735	3.99699E-07
Frem2	-1.18810264	0.000273765
Adap1	-1.189322063	2.01986E-05
Ctps	-1.197481746	2.69883E-15
Susd4	-1.20394234	3.88571E-10
Slc30a2	-1.204099337	0.007381624
Serpinb7	-1.204875062	1.60632E-15
Acot12	-1.207073048	0.003269479
Fam20a	-1.211117792	7.80325E-08
Lmod2	-1.215371078	0.001376363
Osbpl10	-1.216519316	7.01462E-07
Krtap3-1	-1.217224229	0.000503954
Dcp1b	-1.21826797	2.01729E-11
Fxyd4	-1.219256014	0.000597777
Htr1d	-1.21955686	5.48495E-07
Fhod3	-1.221017983	3.63604E-06
Vcan	-1.222285989	9.78274E-06
Rnf180	-1.227192731	0.000566501
Ikzf4	-1.227848918	1.2318E-07

Efemp1	-1.228579612	1.67381E-10
Zfp937	-1.228896517	0.003510394
Tbc1d30	-1.233564609	3.3989E-10
Eid2	-1.239503504	0.003967921
Ahnak2	-1.246124702	1.78972E-11
Prom1	-1.249579058	0.00690114
A530016L24Rik	-1.251391758	0.003546523
Cpm	-1.251830564	4.68948E-05
Col14a1	-1.25435714	6.46595E-06
Cfap70	-1.256422368	0.008473109
Arid3a	-1.257186427	1.72017E-11
Zfp612	-1.257439267	0.000155141
Dclk2	-1.267904706	1.27706E-05
P2ry2	-1.268512874	7.36174E-08
Ccl28	-1.273220812	8.87025E-06
Dennd2a	-1.275290717	0.007416388
Serpinb6d	-1.276831852	1.1035E-05
Lgals7	-1.286379781	5.53721E-05
Il20ra	-1.288294013	0.004822713
Trim15	-1.28862445	0.001979653
Gldc	-1.289697937	0.000151242
D6Ertd527e	-1.297515511	0.002793491
Capn12	-1.297978716	3.78151E-12
Tspan7	-1.298739905	1.65753E-14
Cdkn1c	-1.306040553	0.004962898
Eln	-1.308012012	0.00056953
Zfp608	-1.316022735	2.74671E-07
Cyp2b23	-1.316932038	6.53537E-06
Ica1l	-1.320641656	0.000970042
Aldh3b3	-1.325540724	7.10532E-16
Clec2e	-1.329606349	0.000119398
Ptger3	-1.331859146	0.000145842
Smad9	-1.333999258	0.000476068
F3	-1.335917542	2.28164E-18
Acvr2b	-1.34021805	0.009751475
Lonrf3	-1.340231513	0.000200543
Zfhx2	-1.344243102	1.48525E-07
Prss53	-1.345172883	1.47884E-06
Ephb1	-1.345770007	0.0006656
Pdia5	-1.351434904	0.000636776
Rpp25	-1.353788661	0.000761341
Fmo1	-1.360063269	5.99145E-05
Chd5	-1.360843632	0.007100269
Svip	-1.368117026	2.64015E-08

Cygb	-1.369908462	8.55287E-05
Mgat5b	-1.374495781	3.95173E-06
Lrat	-1.376488908	0.000979439
Cilp	-1.37876731	0.005357691
Mfsd4	-1.388034902	3.70109E-10
Sod3	-1.3901562	0.005111228
Pde1c	-1.398472994	0.000148662
Sulf1	-1.407431916	0.003141655
Lmtk3	-1.411268838	0.000244474
D730001G18Rik	-1.411619181	0.000818573
Psors1c2	-1.412281331	9.13045E-10
Ccdc69	-1.413242859	0.003910513
Gm13177	-1.416402175	7.27973E-11
Entpd3	-1.42432949	1.05853E-06
Tacr3	-1.430759684	0.000236258
Palm3	-1.432162325	2.59466E-06
Igfbp5	-1.440220178	9.84189E-06
Foxc2	-1.443502975	1.1035E-05
Hmgn2	-1.446368327	0.00640313
Tnfrsf13c	-1.45200694	4.83181E-05
Cd19	-1.458543859	0.002601025
Rasd2	-1.460183252	0.000152995
Cybrd1	-1.46350546	3.00325E-08
Nup210	-1.473790262	1.4021E-09
Dlx4	-1.475420392	3.47776E-09
Gm11569	-1.486852988	0.005865179
Cacna1d	-1.486882236	7.98147E-05
Ccdc109b	-1.493573758	3.0162E-06
Nmnat2	-1.495509865	0.000483754
Slc4a9	-1.510390596	5.62747E-08
Tll1	-1.513240696	0.000752587
Hpgd	-1.517110808	6.62252E-23
Trpm6	-1.518664171	0.000730397
Lrrc31	-1.519827096	0.000296831
Cysltr1	-1.520042339	0.001324746
Krt32	-1.521351633	0.002693656
Nkd1	-1.521447317	7.48229E-09
Lppr3	-1.524055367	1.22967E-09
Igfbp3	-1.524854196	5.62097E-05
Rab37	-1.527502746	0.001321488
Kcne1	-1.528114151	0.008993478
Sstr2	-1.530415749	0.002692875
Mex3a	-1.533068876	7.99085E-15
Plce1	-1.535365014	0.002630921

Cdh4	-1.538582835	1.4661E-05
Pde9a	-1.538920623	0.000647817
Gja1	-1.54177872	6.96801E-10
Coro6	-1.550953097	0.00438051
Fras1	-1.55485205	8.11599E-05
Slc5a5	-1.5570641	0.000290651
Selenbp2	-1.557330487	9.82796E-20
Gpr176	-1.557538995	0.000182769
Gatm	-1.562184606	2.49303E-06
Kcng2	-1.567500991	0.001566227
Ifi205	-1.568025485	0.001438505
Mest	-1.57108776	1.17898E-05
Cldn8	-1.571891363	4.74167E-12
Tspear	-1.579852227	0.000309069
Mtcl1	-1.586258209	6.28913E-11
Ebf4	-1.58816803	0.001139128
Krtap3-3	-1.588324369	0.000148329
Bambi	-1.590090658	1.85066E-10
Nim1k	-1.598537043	1.11383E-05
Pvrl3	-1.600752699	0.000133938
Elf5	-1.60187165	5.01557E-09
Cystm1	-1.602810345	2.0344E-09
Adamts14	-1.604745681	2.5401E-15
Srms	-1.613312405	2.1157E-07
Ldoc1l	-1.620784883	6.00469E-06
Snhg11	-1.622432128	3.40226E-08
Ccr4	-1.62716433	7.57885E-05
Hecw2	-1.631533382	7.71759E-05
Krt73	-1.632066943	0.00250614
Hspa12a	-1.633361509	3.26361E-19
Spock2	-1.637455199	6.9067E-28
Fam228b	-1.637735442	0.000741722
Xpnpep2	-1.637800707	6.37555E-06
Slc18a1	-1.637985633	0.000348099
Smc1b	-1.642184402	0.004502668
Gpr156	-1.648313735	1.70531E-05
Msx1	-1.648907036	5.07508E-05
Krt28	-1.651752676	0.001385896
Tmem28	-1.652916397	7.54241E-07
Golga7b	-1.658301288	8.77596E-06
Slc38a3	-1.658751366	7.08425E-07
Ceacam1	-1.661351594	0.003847129
Muc3a	-1.666817043	5.75245E-05
Rassf2	-1.680382382	1.90635E-05

Ccdc149	-1.684245748	2.19212E-05
Gnmt	-1.685263422	0.000455343
Igf2	-1.689140615	0.000142777
Slc4a1	-1.689351182	0.00079114
Tchh	-1.698076959	0.000969344
Bean1	-1.698792328	0.000587802
Gabrp	-1.706250344	0.000424397
Fgd5	-1.707700753	0.005471903
Ccdc158	-1.713530059	0.000671563
Cxxc4	-1.718619132	0.000132519
Ugt2b1	-1.72531576	0.005944941
Fam49a	-1.73516181	7.9917E-07
Krt71	-1.740036414	0.002466243
Xkr6	-1.743145304	1.45002E-09
Dclk3	-1.74438736	0.000144549
Zfp941	-1.744776486	0.000707279
Fndc4	-1.747045457	4.50096E-07
Cldn10	-1.751819926	6.27798E-06
Ablim2	-1.75743324	5.78836E-05
Steap1	-1.760316056	7.55609E-06
Slc39a8	-1.772190206	0.000357038
Gpm6a	-1.783744612	5.32781E-14
Mpo	-1.786283145	0.002815094
Kcp	-1.791798205	0.00261773
Pm20d1	-1.792782934	4.29066E-32
Upp1	-1.794079184	0.000411853
Mlf1	-1.798030263	3.22543E-14
Eml1	-1.799087089	7.228E-16
Cryba4	-1.799203605	0.001570645
Gm7735	-1.803622532	7.60444E-06
Myb	-1.803923925	1.81192E-07
Chac1	-1.807587136	7.40378E-16
Heyl	-1.811321626	0.002983543
Gja3	-1.82001441	6.45954E-08
Fap	-1.826744309	0.000466863
Fam124b	-1.82786417	4.3521E-07
Oprd1	-1.829627351	0.000843694
En1	-1.831600624	0.000513164
Scn4b	-1.832181743	2.1662E-05
Krtap27-1	-1.837078961	5.62097E-05
Bend5	-1.837536604	7.39518E-10
Krtap6-2	-1.847137771	1.72425E-08
Nxf7	-1.863366871	0.000181181
Olfml2b	-1.870643331	7.29165E-05

Mal	-1.870969017	8.00963E-06
Gm11554	-1.873472031	9.66221E-05
Reep1	-1.874819019	1.96046E-09
Gng4	-1.875233941	1.23186E-07
Eci3	-1.878727648	0.004699534
Ccnjl	-1.884392048	0.002805295
Scara5	-1.889100139	0.002568308
Gpr50	-1.890283864	2.20156E-05
Akap12	-1.890442472	7.39587E-07
Prrt1	-1.892076949	9.07556E-06
Nsg1	-1.892202444	1.72017E-11
Lef1	-1.893027933	4.38852E-09
Slc35f1	-1.893135932	5.43272E-07
Ly6g6d	-1.899686778	0.000128716
Msx2	-1.903144918	6.28913E-11
Myef2	-1.913418783	8.26722E-11
Krtap20-2	-1.914210347	6.96535E-12
Gm11564	-1.915940802	0.000781316
Mettl7a3	-1.922357452	1.97263E-06
Gfra3	-1.922536107	5.4051E-07
Krt27	-1.932209761	0.001183934
Nrxn2	-1.936190215	1.97531E-07
Krtap3-2	-1.943491018	3.80019E-10
Gfra2	-1.945310721	0.000208649
Dysf	-1.952866494	2.46299E-08
St8sia6	-1.958887778	1.42421E-05
Dnajc6	-1.960123395	4.65883E-09
Procr	-1.967369513	1.01274E-06
B4galnt4	-1.974211793	7.36536E-11
Adrb1	-1.978425781	2.18331E-07
Rgs6	-1.982074848	0.000752728
2310079G19Rik	-1.993246612	0.001544723
Gm438	-2.002058479	1.68475E-22
Krt39	-2.005277415	2.47386E-06
Atp8b5	-2.016909843	0.001124375
Ccdc155	-2.022692603	3.99699E-07
S100a3	-2.030793533	0.000107123
Fbp1	-2.03307297	0.000375002
Cldn14	-2.034918745	0.000407135
Gm9833	-2.035634706	2.11812E-06
Galnt9	-2.044729375	5.50884E-06
Gpc3	-2.045372652	3.15545E-18
Serpina1e	-2.062081639	0.000739572
Dusp2	-2.063991397	2.79614E-07

Stox1	-2.07441413	7.50024E-05
Il1f10	-2.081587466	3.55642E-08
Gprc5a	-2.082290598	5.18776E-05
Bhlha9	-2.090391028	0.000688413
Efhd1	-2.095352116	9.61603E-11
Zfp618	-2.099872091	2.45477E-39
Ctse	-2.102691496	9.73026E-05
Fam169a	-2.118579894	0.000682774
Nkd2	-2.128456488	3.26968E-07
Prdm8	-2.131090129	0.001838085
Pcp4	-2.134890436	8.30587E-07
Myo5c	-2.143510814	6.1443E-09
Slc9a2	-2.149807462	4.57792E-05
Tigd4	-2.151579783	6.5039E-08
Gm10228	-2.172046743	1.0121E-09
Krt82	-2.182144456	0.00363494
Rnf182	-2.193947642	2.98102E-06
Dsg4	-2.196393593	0.000156479
Krtap6-1	-2.219588854	5.02769E-07
Skint11	-2.227419012	2.04669E-10
Lrrc15	-2.238065612	1.92437E-10
Krtap16-1	-2.238163589	0.001130784
Krtap9-5	-2.239650443	3.16972E-06
Krtap24-1	-2.239869449	0.002094061
Padi1	-2.24143625	2.3848E-06
Prr9	-2.248166713	2.04709E-11
Npy1r	-2.262725708	1.98863E-06
Krt74	-2.275954929	5.55206E-07
Padi3	-2.280068506	0.000244363
Krtap21-1	-2.283547921	3.51027E-10
Csdc2	-2.295905398	3.60766E-09
S100a7a	-2.296041996	1.39135E-08
Rgs16	-2.296596239	2.1383E-05
Krt40	-2.321606551	0.000600181
Krtap17-1	-2.321898671	1.27436E-06
Pkdrej	-2.323794459	0.000107979
Rtkn2	-2.346184154	1.2987E-08
Sptssb	-2.35403826	7.1994E-07
Krtap13-1	-2.369384887	2.46055E-07
Syt7	-2.382621131	6.68065E-09
Tesc	-2.384053329	2.87323E-15
Il22ra2	-2.384254895	4.82479E-09
Capn8	-2.384773319	2.89226E-07
Bmp8a	-2.386111335	9.75131E-08

Scgb1a1	-2.389153574	2.16994E-18
Krtap6-5	-2.390259491	1.40149E-09
Bex1	-2.39735538	1.04619E-05
Chrna4	-2.411209551	0.000834734
Crnn	-2.415867222	2.97211E-08
Zpbp	-2.436588443	1.90635E-05
Krt25	-2.439247604	0.000820776
Vsig8	-2.445733594	0.000370171
Krt26	-2.454577579	0.000414244
1110025L11Rik	-2.470151097	1.3995E-07
Itga11	-2.477444422	1.42646E-05
Grm4	-2.481652115	2.10802E-10
Gm3250	-2.488278754	1.11416E-08
Krtap22-2	-2.489617149	2.1348E-10
Krt72	-2.489701735	0.000148852
Krtap26-1	-2.492125566	3.34894E-06
Krtap10-4	-2.502256535	0.000246438
Lyg2	-2.50701389	0.000933096
Foxl1	-2.514146811	0.001545073
Tmprss11c	-2.519929246	0.00043496
Klk15	-2.52368422	6.87658E-08
Sez6	-2.531976297	0.002767117
Gm3233	-2.534882924	9.14251E-06
Crym	-2.552400659	4.79172E-06
Gm7138	-2.555380012	1.85066E-10
Krt31	-2.575171731	6.37958E-05
Krtap4-16	-2.581645002	2.25559E-05
Gm3238	-2.587727845	6.43614E-05
Actbl2	-2.594303484	2.34394E-05
Slco4c1	-2.597861113	4.97553E-05
Krt34	-2.599388566	9.78274E-06
Kcnk16	-2.636296702	8.8273E-05
Gm11562	-2.641350221	2.84632E-09
Pla2g4c	-2.646173198	9.03207E-15
Fam26d	-2.647676767	0.000209221
5430421N21Rik	-2.648366982	6.43301E-06
Krt83	-2.650453549	1.43813E-06
Gm10272	-2.654932496	7.60444E-06
Krt86	-2.671458891	1.06086E-05
Fabp4	-2.693339413	1.49004E-12
Slc13a2	-2.693614521	0.006699166
Gm10229	-2.695501376	1.38824E-09
Csmd2	-2.704266096	0.000130488
Grik4	-2.704428864	1.36979E-19

Gm10142	-2.707049729	1.79872E-06
Krtap11-1	-2.710909734	1.72766E-05
Rgs7bp	-2.723712428	1.97531E-07
Car8	-2.727010765	1.42708E-05
Gm11938	-2.745562606	6.11973E-08
Krtap4-8	-2.747906331	1.5101E-07
Krtap4-9	-2.748577738	4.59821E-07
Krtap19-5	-2.75142545	1.51539E-08
Gm11937	-2.754419141	1.2183E-07
Cpxm2	-2.764628007	4.65735E-50
Krtap12-1	-2.77128549	1.1035E-05
Krt81	-2.774425057	4.12154E-06
Gm266	-2.776176381	2.54558E-10
Dio3	-2.77941411	1.34521E-11
Adamts19	-2.784471759	2.63997E-05
Pax7	-2.788219434	4.83181E-05
Krtap2-4	-2.788916728	5.77165E-08
Gm19402	-2.791499326	6.8247E-06
Gm11939	-2.798583318	9.91565E-19
Tagln3	-2.799229629	4.87383E-08
Gm9507	-2.80438723	8.87864E-05
Krt33b	-2.809277596	8.9707E-06
Gm10024	-2.825292875	7.08568E-05
Gm11595	-2.854793187	6.63124E-08
Gm11596	-2.857677717	4.33668E-08
Gm19668	-2.858712033	1.50898E-06
Gprc5d	-2.871884753	7.1994E-07
Krtap4-2	-2.876686498	3.17171E-08
Krtap1-3	-2.879373593	5.7069E-07
Syt17	-2.890451029	6.51568E-10
Krtap29-1	-2.895859207	2.22911E-09
Skint6	-2.900927483	2.24804E-23
Tchhl1	-2.907731533	1.50725E-10
Gm11568	-2.908526281	1.29009E-06
Krtap4-7	-2.91398894	1.78054E-07
Gm7137	-2.916935428	1.60793E-11
Cacna1i	-2.924081905	1.49045E-05
Mcpt1	-2.929058195	2.68907E-06
Gm11563	-2.950776363	7.54361E-08
Krtap1-4	-2.950894008	3.75498E-07
Slc26a3	-2.95610856	1.30539E-05
Slco5a1	-2.961304037	6.33496E-08
Tm4sf4	-2.973220132	3.39684E-07
Myom2	-2.976942234	4.24932E-14

Krt33a	-2.988912655	1.48924E-05
Prr5l	-3.00190194	1.40801E-12
Krtap9-3	-3.002199979	1.92628E-07
Gm11555	-3.038827069	1.0316E-08
Krtap4-1	-3.048323868	6.66748E-08
Krtap19-4	-3.070748245	4.21077E-07
Ifitm6	-3.076503284	1.85044E-05
Krtap4-13	-3.082121515	4.20477E-11
Gm10100	-3.112213951	3.62528E-07
Krtap6-3	-3.139561986	1.17596E-15
Cdh6	-3.158513135	6.65201E-10
Krtap4-6	-3.171133216	5.10367E-09
Gm11559	-3.1897993	7.31455E-07
Gm9789	-3.266386675	9.38716E-15
Gm11567	-3.294143605	9.75131E-08
Kcnn3	-3.29895543	0.000196629
Krtap9-1	-3.323377576	1.57182E-07
Krtap8-1	-3.416045085	1.8243E-10
Slc6a13	-3.417379874	1.14647E-09
Krtap19-3	-3.430161668	5.45638E-10
Krtap14	-3.440406152	9.09171E-08
Krtap15	-3.478945133	5.54133E-07
Krtap1-5	-3.491914134	8.71638E-10
Crisp1	-3.510979271	0.00010015
Krtap19-9b	-3.523189558	3.4226E-09
Apba2	-3.535020946	7.33937E-14
0610040J01Rik	-3.539111308	3.34626E-21
Krtap31-1	-3.539655678	7.10884E-14
Krtap19-9a	-3.580508701	8.35191E-12
Krtap7-1	-3.589561545	1.79772E-12
Gadl1	-3.615695474	6.58278E-18
Ccdc80	-3.639550869	4.37034E-26
Krtap19-2	-3.664810219	5.74446E-07
Gm6358	-3.666610846	3.54636E-15
1110057P08Rik	-3.681039574	9.25208E-41
Gm11565	-3.681376756	1.63051E-21
Krtap16-3	-3.727720341	1.11493E-10
Gm10153	-3.757762644	2.20536E-17
Krtap5-5	-3.769537723	3.99624E-08
Krtap19-1	-3.844610307	4.38272E-09
Krtap5-3	-3.847258335	7.91006E-10
Krtap5-2	-3.856372316	3.23441E-10
Krtap28-13	-3.963397758	1.5323E-08
Gm4553	-3.970478793	1.07964E-29

Stk33	-3.987568342	1.45121E-08
Gm4559	-3.992923633	3.4901E-21
Gm2431	-4.058621123	1.07964E-29
Krtap31-2	-4.14950965	2.16359E-18
Krtap5-4	-4.160511689	6.96535E-12
Rasgrf2	-4.232670612	6.77847E-26
Ogn	-4.244275854	9.2366E-46
Krtap5-1	-4.296088346	9.67429E-31
Hhip	-4.364200841	1.88577E-31
Skint9	-6.745196022	7.72867E-52
Skint3	-7.298019329	4.29114E-75
Skint4	-7.504350272	1.72776E-81

SUPPLEMENTARY TABLE S5: Downregulated DEGs (SKOvsCTR) are enriched for *Krt* and *Krtap* genes.

Gene name	SKOvsCTR : logFC	SKOvsCTR : FDR
Krtap5-1	-4.296088346	9.67429E-31
Krtap5-4	-4.160511689	6.96535E-12
Krtap31-2	-4.14950965	2.16359E-18
Krtap28-13	-3.963397758	1.5323E-08
Krtap5-2	-3.856372316	3.23441E-10
Krtap5-3	-3.847258335	7.91006E-10
Krtap19-1	-3.844610307	4.38272E-09
Krtap5-5	-3.769537723	3.99624E-08
Krtap16-3	-3.727720341	1.11493E-10
Krtap19-2	-3.664810219	5.74446E-07
Krtap7-1	-3.589561545	1.79772E-12
Krtap19-9a	-3.580508701	8.35191E-12
Krtap31-1	-3.539655678	7.10884E-14
Krtap19-9b	-3.523189558	3.4226E-09
Krtap1-5	-3.491914134	8.71638E-10
Krtap15	-3.478945133	5.54133E-07
Krtap14	-3.440406152	9.09171E-08
Krtap19-3	-3.430161668	5.45638E-10
Krtap8-1	-3.416045085	1.8243E-10
Krtap9-1	-3.323377576	1.57182E-07
Krtap4-6	-3.171133216	5.10367E-09
Krtap6-3	-3.139561986	1.17596E-15
Krtap4-13	-3.082121515	4.20477E-11
Krtap19-4	-3.070748245	4.21077E-07
Krtap4-1	-3.048323868	6.66748E-08
Krtap9-3	-3.002199979	1.92628E-07
Krt33a	-2.988912655	1.48924E-05
Krtap1-4	-2.950894008	3.75498E-07
Krtap4-7	-2.91398894	1.78054E-07
Krtap29-1	-2.895859207	2.22911E-09
Krtap1-3	-2.879373593	5.7069E-07
Krtap4-2	-2.876686498	3.17171E-08
Krt33b	-2.809277596	8.9707E-06
Krtap2-4	-2.788916728	5.77165E-08
Krt81	-2.774425057	4.12154E-06
Krtap12-1	-2.77128549	1.1035E-05
Krtap19-5	-2.75142545	1.51539E-08
Krtap4-9	-2.748577738	4.59821E-07
Krtap4-8	-2.747906331	1.5101E-07
Krtap11-1	-2.710909734	1.72766E-05
Krt86	-2.671458891	1.06086E-05
Krt83	-2.650453549	1.43813E-06

Krt34	-2.599388566	9.78274E-06
Krtap4-16	-2.581645002	2.25559E-05
Krt31	-2.575171731	6.37958E-05
Krtap10-4	-2.502256535	0.000246438
Krtap26-1	-2.492125566	3.34894E-06
Krt72	-2.489701735	0.000148852
Krtap22-2	-2.489617149	2.1348E-10
Krt26	-2.454577579	0.000414244
Krt25	-2.439247604	0.000820776
Krtap6-5	-2.390259491	1.40149E-09
Krtap13-1	-2.369384887	2.46055E-07
Krtap17-1	-2.321898671	1.27436E-06
Krt40	-2.321606551	0.000600181
Krtap21-1	-2.283547921	3.51027E-10
Krt74	-2.275954929	5.55206E-07
Krtap24-1	-2.239869449	0.002094061
Krtap9-5	-2.239650443	3.16972E-06
Krtap16-1	-2.238163589	0.001130784
Krtap6-1	-2.219588854	5.02769E-07
Krt82	-2.182144456	0.00363494
Krt39	-2.005277415	2.47386E-06
Krtap3-2	-1.943491018	3.80019E-10
Krt27	-1.932209761	0.001183934
Krtap20-2	-1.914210347	6.96535E-12
Krtap6-2	-1.847137771	1.72425E-08
Krtap27-1	-1.837078961	5.62097E-05
Krt71	-1.740036414	0.002466243
Krt28	-1.651752676	0.001385896
Krt73	-1.632066943	0.00250614
Krtap3-3	-1.588324369	0.000148329
Krt32	-1.521351633	0.002693656
Krtap3-1	-1.217224229	0.000503954

SUPPLEMENTARY TABLE S6: Overlap of upregulated DEGs (SKOvsCTR) and the GO_Immune_System_Process gene set.

Gene name	SKOvsCTR : logFC	SKOvsCTR : FDR
Ccl2	5.569476383	2.4143E-32
Ccl1	4.96704325	2.31247E-33
S100a9	4.622518139	1.43652E-10
Ccl20	4.228922878	4.66147E-23
S100a8	4.174235752	5.45686E-11
Pglyrp2	4.100906903	5.13833E-45
Blk	3.385207475	9.2625E-09
Cxcl10	3.2093752	1.16146E-08
Tnfsf4	3.157810331	8.93336E-05
Icos	3.025441396	0.000115095
Cxcl9	2.988683416	0.000689781
Il2rg	2.924128947	5.27519E-08
Ltb	2.917122347	7.03577E-06
Ccr2	2.906344841	2.25655E-08
Epb42	2.879079741	8.41099E-07
Gbp2	2.861369161	1.03382E-06
Cxcl1	2.837231096	7.51794E-07
Il18r1	2.821486218	1.32664E-17
Ccl7	2.818406405	0.000224406
Cd247	2.7702066	6.69687E-06
Igsf6	2.640476991	1.96569E-05
Cd3e	2.608574217	1.26872E-05
Ctsk	2.583007451	0.00012796
Il18rap	2.43188571	6.72608E-06
Tnf	2.364621827	2.13605E-06
Slc16a3	2.331840536	3.83735E-22
Pmaip1	2.270588654	7.92366E-09
Lax1	2.231451207	2.10887E-20
Mmp9	2.21669885	2.68206E-10
Lcn2	2.114326884	3.1714E-10
Slpi	2.062517659	5.56526E-12
Casp4	2.037305091	0.000272302
Artn	2.033294683	2.40136E-07
Mx1	1.989569898	9.55259E-05
Chga	1.940190275	3.60766E-09
Lif	1.870071066	4.10946E-07
Il7r	1.867356535	1.58689E-08
Dock2	1.719123784	0.000113138
Nlrc5	1.710007555	9.31974E-21
Fgr	1.543307444	0.002954787
Krt1	1.540248096	0.000161752
Rltpr	1.536677471	0.001873894

Ets1	1.524817188	2.04355E-13
Ccr1	1.514548667	0.001077273
Psmb9	1.507861764	5.86659E-07
Vcam1	1.481892988	0.000570118
Itgb7	1.477629277	0.000424397
Krt16	1.473964756	4.92006E-11
Psmb8	1.468655102	4.8278E-13
Fcgr2b	1.459207252	0.000407716
Hsp90ab1	1.458004795	3.07521E-09
Il1f6	1.447659593	3.27643E-10
Fst	1.442738865	2.5538E-14
Notch4	1.421053645	0.000154891
B2m	1.379895788	9.01899E-16
Coro1a	1.378541738	4.59076E-06
Klf2	1.36067873	0.000463746
Gsdmd	1.318862445	0.000324693
Tbkbp1	1.286445136	6.95766E-05
Ctss	1.281983114	2.32335E-05
C1rl	1.253907743	1.23164E-05
Kcnab2	1.232263077	0.001323203
Isg15	1.229937075	0.004799382
Ly75	1.184912412	2.30916E-05
Fas	1.177586048	0.001065651
Cyba	1.175404835	0.000487845
Tnfsf18	1.173972425	0.002649254
Lat	1.169941928	0.006626504
Itgax	1.162489042	0.000340789
Irf1	1.152309193	1.33336E-06
Anxa3	1.14686161	3.09785E-06
Selplg	1.139932891	3.85628E-05
Spn	1.1251528	0.000638154
Lgals9	1.12183177	6.86959E-09
Lcp1	1.114584033	6.20328E-05
Tnfrsf25	1.114468972	0.000434425
Csf1	1.113633752	0.000200065
Nckap1l	1.09836085	0.000861462
Serpinb12	1.095479028	3.29726E-06
Cxcl16	1.083921222	7.89148E-10
Tmem173	1.0677548	0.004052918
Tap2	1.061812691	5.34864E-10
H2-Eb1	1.042248308	8.26218E-07
Pglyrp3	1.040281782	0.000108119
Jak3	1.039237981	0.000487845
Il1f5	1.031253951	1.08214E-07

Icam1	1.030354606	2.55228E-07
Serpinb9	1.027089861	0.008812934
Il33	1.004278997	0.000204035
Ccl22	1.001835942	4.66887E-06